



Published in final edited form as:

Cell. 2018 May 17; 173(5): 1083–1097.e22. doi:10.1016/j.cell.2018.04.006.

Blocking neuronal signaling to immune cells treats streptococcal invasive infection

Felipe A. Pinho-Ribeiro¹, Buket Baddal², Rianne Haarsma¹, Maghnus O'Seaghda^{2,3}, Nicole J. Yang¹, Kimbria J. Blake¹, Makayla Portley¹, Waldiceu A. Verri Jr⁴, James B. Dale⁵, Michael R. Wessels², and Isaac M. Chiu^{1,*†}

¹Division of Immunology, Department of Microbiology and Immunobiology, Harvard Medical School, Boston, MA, 02115, USA

²Division of Infectious Diseases, Boston Children's Hospital, and Department of Pediatrics, Harvard Medical School, Boston, MA, 02115, USA

³Department of Biology, Suffolk University, Boston, MA, 02108, USA

⁴Departamento de Ciências Patológicas, Centro de Ciências Biológicas, Universidade Estadual de Londrina, Londrina, PR, 10011, Brazil

⁵Department of Medicine, Division of Infectious Diseases, University of Tennessee Health Science Center, Memphis, TN, 38163, USA

SUMMARY

The nervous system, the immune system, and microbial pathogens interact closely at barrier tissues. Here we find that a bacterial pathogen, *Streptococcus pyogenes*, hijacks pain and neuronal regulation of the immune response to promote bacterial survival. Necrotizing fasciitis is a life-threatening soft tissue infection in which “pain is out of proportion” to early physical manifestations. We find that *S. pyogenes*, the leading cause of necrotizing fasciitis, secretes streptolysin S (SLS) to directly activate nociceptor neurons and produce pain during infection. Nociceptors, in turn, release the neuropeptide calcitonin gene-related peptide (CGRP) into infected tissues, which inhibits the recruitment of neutrophils and opsonophagocytic killing of *S. pyogenes*. Botulinum neurotoxin A and CGRP antagonism block neuron-mediated suppression of host defense, thereby preventing and treating *S. pyogenes* necrotizing infection. We conclude that targeting the peripheral nervous system and blocking neuro-immune communication is a promising strategy to treat highly invasive bacterial infections.

[†]Lead Contact and ^{*}Correspondence to: Isaac M. Chiu, Department of Microbiology and Immunobiology, Harvard Medical School, 77 Avenue Louis Pasteur, Boston, MA, 02115, USA., Phone: (617) 432-1236, isaac_chiu@hms.harvard.edu.

Publisher's Disclaimer: This is a PDF file of an unedited manuscript that has been accepted for publication. As a service to our customers we are providing this early version of the manuscript. The manuscript will undergo copyediting, typesetting, and review of the resulting proof before it is published in its final citable form. Please note that during the production process errors may be discovered which could affect the content, and all legal disclaimers that apply to the journal pertain.

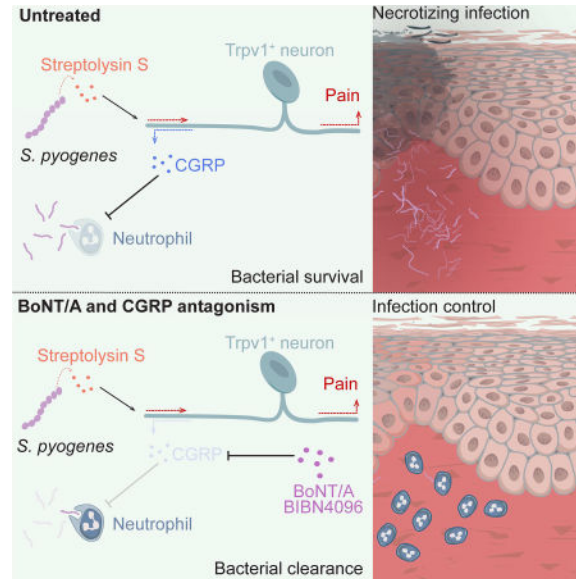
AUTHOR CONTRIBUTIONS

Conceptualization, FAPR, IMC, MRW; Construction of unique reagents and bacterial strains, JD, BB, MO; Experimentation and data analysis, FAPR, BB, RH, MO, NJY, KJB, MP; Writing-original draft, FAPR, IMC; Review/editing manuscript, FAPR, BB, WAVJ, MRW, IMC; Funding acquisition, WAVJ, MRW, IMC.

DECLARATION OF INTERESTS

FAPR, BB, NJY, MRW and IMC are co-inventors on patents that incorporate discoveries described in the manuscript.

IN BRIEF



Flesh-eating bacteria hijack a pain response that suppresses host defense and blocking this neuro-immune communication holds potential for treatment

The skin is a major barrier tissue that is exposed to external insults and microbial invasion. The somatosensory nervous system densely innervates the skin, detecting noxious and environmental stimuli to mediate pain, itch, thermosensation, and mechanosensation (Abraira and Ginty, 2013; Basbaum et al, 2009). Somatosensory neurons actively communicate with the immune system in pain and inflammatory conditions (Pinho-Ribeiro et al., 2017). However, the role of the sensory nervous system in host defense is not well understood. Here we find that *Streptococcus pyogenes*, an invasive bacterial pathogen, activates sensory neurons to produce pain and to induce neural suppression of the immune system to enhance its survival during infection.

Necrotizing fasciitis (or “flesh-eating disease”) is a life-threatening, aggressive bacterial infection of the subcutaneous tissue and underlying fascia. A cardinal manifestation of this infection is “pain out of proportion” to physical findings at early time points (Borschitz et al., 2015). *S. pyogenes* (or group A *Streptococcus*) is a gram-positive bacterial pathogen and the leading cause of necrotizing fasciitis (Leitch et al., 2000). *S. pyogenes* also frequently causes pharyngitis (or “strep throat”), a painful infection that affects 600 million people annually (Ralph and Carapetis, 2013). Necrotizing fasciitis is difficult to treat and has a mortality rate of 24–32% in developed countries (Cole et al., 2011). Due to its rapid progression, disfiguring surgical debridement or limb amputation is often required to prevent mortality. Despite the importance of pain in the diagnosis of necrotizing fasciitis, the role of pain in *S. pyogenes* invasion is unclear.

Nociceptor neurons are the specific subset of peripheral sensory neurons that mediate pain, an unpleasant sensation that warns organisms of danger. In addition to transducing pain

signals to the central nervous system, nociceptors release neuropeptides from their peripheral nerve terminals that can directly modulate inflammation. These neuropeptides bind to their cognate receptors on immune cells, leading to changes in transcription, cytokine production, and immune phenotypic polarization (Pinho-Ribeiro et al., 2017). Recent work shows that sensory neurons communicate with immune cells in allergic airway inflammation (Caceres et al., 2009; Talbot et al., 2015), atopic dermatitis (Wilson et al., 2013a, 2013b; Oetjen et al., 2017), and psoriasis (Riol-Blanco et al., 2014).

We identify a critical role for the nervous system in the regulation of host defense during *S. pyogenes* invasive infection. In mouse models of necrotizing fasciitis established using *S. pyogenes* clinical isolates, we show that bacteria directly activate TRPV1⁺ neurons to produce pain through the action of the secreted pore-forming toxin SLS. Nociceptors release CGRP, a neuropeptide that suppresses the recruitment and bactericidal activity of neutrophils essential for host defense. Silencing nerve fibers and their signaling to immune cells via administration of botulinum neurotoxin A (BoNT/A) or a CGRP antagonist halts bacterial invasion, showing that targeting the nervous system could be a strategy to enhance host defense and treat invasive bacterial infections.

RESULTS

S. pyogenes induces pain independently of the inflammatory response

To study the role of pain fibers in bacterial invasion, we adapted a mouse model of *S. pyogenes* infection shown to mimic pathologic features of human necrotizing fasciitis (Ashbaugh et al., 1998). We used two *S. pyogenes* strains from human infections: 1) 854 M-type 1 (M1), a clinical isolate representative of the dominant clonal group among isolates from contemporary invasive infections (Gryllos et al., 2008), and (2) 950771 M-type 3 (M3), a clinical isolate from a child with necrotizing fasciitis (Ashbaugh et al., 1998).

We initiated subcutaneous infection of the mouse hind paw, which is densely innervated and well suited for the study of pain reflex behaviors. Both bacterial strains induced progressive edema and dermonecrotic lesions (Figure 1A), necrosis in the subcutaneous tissues, overlying dermis, and thrombosis of the arterioles and venules, resembling human necrotizing fasciitis (Figure 1B). Body weight loss and mortality occurred over time, associated with bacterial proliferation (Figure S1A–S1C). While M3 produced lethality at all doses, M1 only caused death at the highest dose (Figure S1B).

Pain behavioral analysis showed that both *S. pyogenes* M1 and M3 bacterial strains evoked dose-dependent and robust, spontaneous lifting/licking and flinching pain reflexes of the infected paw within minutes of injection (Figures 1C, S1D–S1E). M1 and M3 strains also produced dose-dependent mechanical hyperalgesia (increased sensitivity to noxious stimuli) within 1 h that continued for 48 h post-injection (Figure 1D). At lower doses, M1 infection induced stronger mechanical hyperalgesia than M3 infection. Heat hyperalgesia was also robustly produced by *S. pyogenes* M1 and M3 in a similar time course as mechanical hyperalgesia (Figure 1E). Because mechanical and heat sensitivity returned towards baseline at 48 h after infection (Figure 1D–1E), we determined if this transition was correlated with neural damage. At 48 h and 72 h post-infection, we did not detect significant changes in the

proportions of TRPV1+, CGRP+, or NF200+ cell bodies in the L4–L6 dorsal root ganglia (DRG) (Figure S1F). However, we detected loss of sensory nerve fibers innervating the footpad in mice infected with M1 *S. pyogenes* at 72 h. At the center of infected lesions, there was complete loss of CGRP+ and PGP9.5+ nerves, with some intact nerves at lesion borders, whereas nerves remained unaffected in areas remote from the lesion (Figure S1G). Thus, *S. pyogenes* infection induces significant spontaneous pain and hyperalgesia at early time points, as well as subsequent local loss of sensory nerves.

We next determined whether inflammatory mediators or immune cells drove the early intense hyperalgesia during *S. pyogenes* infection. Ibuprofen, which blocks cyclooxygenase mediated prostaglandin synthesis, had no effect on mechanical or heat hyperalgesia (Figure S2A). We next found that mice deficient in caspase-1 (*Casp1*^{-/-}), which mediates IL-1 β production, or mice deficient in myeloid derived factor 88 (*Myd88*^{-/-}), which mediates toll-like receptor and IL-1R signaling, developed hyperalgesia similar to wild-type mice following *S. pyogenes* infection (Figure S2A). Neither depletion of neutrophils (Gr1 antibody treatment), nor deficiency in recombination activating gene 2 (*Rag2*^{-/-}), which mediates T and B cell development, altered the development of hyperalgesia after infection (Figure S2A). These data, together with the observation that *S. pyogenes* induces pain within minutes, suggest that bacteria may directly interact with neurons independent of the immune response.

***S. pyogenes* directly activates nociceptor neurons through SLS**

We next determined whether *S. pyogenes* could directly act on sensory neurons to produce pain. Live M3 *S. pyogenes* induced robust calcium influx in DRG neurons *in vitro* within minutes of application (Figure 1F). Bacteria-responsive neurons also frequently responded to capsaicin, a ligand for TRPV1, a heat-sensitive ion channel expressed by many nociceptors. At lower bacterial concentrations (5×10^8 – 5×10^9 cfu/mL), more capsaicin-responsive (Cap+) neurons were activated by *S. pyogenes* than capsaicin-unresponsive (Cap-) neurons. At 5×10^{10} cfu/mL, the majority of DRG neurons were activated (Figure 1F). Bacteria-free filtered supernatant from M1 *S. pyogenes* cultures also induced calcium influx in DRG neurons in a dose-dependent manner (Figure 2A). Similar to responses to live bacteria, Cap+ nociceptors were more responsive to supernatants from lower density bacterial cultures than were Cap- neurons (Figure 2A). We observed that DRG neurons with smaller cell body areas were more sensitive to activation by bacterial supernatant than larger-sized neurons (Figure S2B).

We hypothesized that *S. pyogenes* pore-forming toxins (PFT) could be molecular candidates for mediators of neuronal activation, due to their capacity to induce cation influx in mammalian cells (Bentley et al., 2005). *S. pyogenes* produces two PFTs, streptolysin O (SLO) and SLS. We generated M1 and M3 isogenic mutant strains that lacked expression of SLO (*slo*), SLS (*sagA*), or both toxins (*slo sagA*). Supernatant from bacteria deficient in SLS (*sagA* and *slo sagA*) did not induce calcium influx in DRG neurons (Figure 2B–2D). Plasmid complementation of SLS (pDL:*sagA*) into SLS mutant bacteria (*sagA* +pDL:*sagA* and *sagA slo*+pDL:*sagA*) restored the ability of *S. pyogenes* to activate neurons at similar levels as wt bacteria (Figure 2B–2D). SLS (*sagA*) was required for *S.*

pyogenes mediated neuronal activation at both low and high bacterial concentrations for Cap⁻ and Cap⁺ cellular subsets (Figures 2D, S2C–S2D). We also found that *S. pyogenes* mediated release of the neuropeptide CGRP by DRG neurons in a SLS-dependent manner (Figure 2E). LDH release assays showed that this neuropeptide release was unrelated to cell lysis (Figure S3A). SLO activity was intact in wt and *sagA* mutant strains, indicating these effects were specific to SLS (Figure S3B).

SLS is critical for *S. pyogenes*-induced pain and pathogenesis

To determine the role of SLS in pain *in vivo*, mice were infected with wt or mutant *S. pyogenes* strains. Spontaneous lifting/licking pain behaviors were abrogated in mice infected with SLS-deficient bacteria (*sagA* and *slo sagA*) on both M1 and M3 *S. pyogenes* strain backgrounds, but not in mice infected with bacteria deficient in SLO alone (*slo*) (Figure 3A). Spontaneous flinches were abrogated in mice infected with SLS deficient strains (Figure 3B). Paw swelling and bacterial load recovery after infection did not vary between wt and mutant strains post-infection at the 1 hour time point after analysis of spontaneous pain behaviors (Figure S3C–S3D).

We next found that mice infected with SLS mutants (*sagA* or *slo sagA*) did not develop mechanical hyperalgesia, while wt and *slo* strains induced significant mechanical hyperalgesia (Figure 3C). Heat hyperalgesia was not significantly altered by deficiencies in SLS or SLO (Figure 3D). We next determined whether antibody neutralization of SLS affected *S. pyogenes*-induced pain. Mice were treated with a polyclonal antibody against a synthetic peptide encoded by *sagA* (Dale et al., 2002). Anti-SLS, but not control IgG, blocked spontaneous pain behaviors following M3 *S. pyogenes* infection (Figures 3E, S3E). Plasmid complementation with a functional copy of *sagA* (pDL:*sagA*) fully restored spontaneous pain reflexes induced by mutant SLS strains (Figure 3F).

To investigate the role of SLS in mediating *S. pyogenes* pathogenesis during soft tissue infection, we initiated infection by subcutaneous injection of M1 *S. pyogenes* (5×10^6 cfu) into the flank, a model that allows serial measurement of skin lesions over time (Ashbaugh et al., 1998). Dermonecrotic lesions appeared 1 day after injection of wt strain, peaked at day 9, and began to decrease after day 10, while mice infected with *sagA* bacteria did not develop dermonecrotic lesions (Figure S4A). No bacteria were recovered at day 9 from mice infected with *sagA S. pyogenes* (Figure S4B). Local abscesses resolved faster in mice infected with *sagA* bacteria, and weight loss was also dependent on SLS (Figure S4C–S4D). Plasmid complementation of *sagA* bacteria with pDL:*sagA* restored dermonecrosis, bacterial proliferation, abscess formation and weight loss to similar levels as wt bacteria (Figure S4A–S4D).

Ablation of nociceptor neurons improves host control of *S. pyogenes* invasion

Since nociceptor neurons responded directly to SLS, which was crucial for *S. pyogenes* pathogenesis, we investigated whether pain fibers played a role in the outcome of infection. We specifically ablated TRPV1 neurons by crossing *Trpv1-Cre* mice with diphtheria toxin A reporter (*Dta*) mice, which ablates TRPV1-lineage neurons. Heat and mechanical hyperalgesia induced by M1 *S. pyogenes* was eliminated in *Trpv1-Cre/Dta* mice compared

to control littermates (Figure 4A–4B). Infection-induced spontaneous pain reflexes were also reduced in these mice (Figure S4E). Loss of TRPV1⁺ and CGRP⁺ DRG neurons was confirmed by immunostaining (Figure S4F).

We next found that *Trpv1-Cre/Dta* mice developed significantly smaller dermonecrotic lesions and faster weight recovery compared to controls following *S. pyogenes* flank infection (Figure 4E–4F). In a second approach to ablate nociceptors, we treated mice with resiniferatoxin (RTX), a high affinity TRPV1 agonist. RTX treatment abrogated spontaneous pain behaviors, mechanical and heat hyperalgesia induced by *S. pyogenes* infection (Figures 4C–4D, S4G), and led to loss of TRPV1⁺ and CGRP⁺ neurons (Figure S4H). RTX-treated mice developed significantly less dermonecrosis and regained body weight faster than vehicle-treated mice following infection (Figure 4G–4H). Skin abscess sizes in RTX-treated mice also resolved faster (Figure S5A). Histopathologic analysis of skin from RTX-treated mice revealed containment of the bacterial infection within a circumscribed abscess containing polymorphonuclear leukocytes, whereas vehicle-treated animals showed necrosis of the subcutaneous tissues with abundant bacteria and relatively few leukocytes (Figures 5A, S5B). Quantitative cultures confirmed log-fold reductions of *S. pyogenes* in lesions of RTX-treated mice compared to vehicle controls (Figure 5B). *S. pyogenes* was cultured from spleens of vehicle-treated mice on day 9, whereas spleens of RTX-treated mice did not yield detectable bacteria (Figure 5B). Spleen size increased during infection in vehicle-treated mice, but not in RTX-treated mice (Figure S5C).

Neutrophils are essential for *S. pyogenes* clearance and prevention of bacterial dissemination (Hidalgo-Grass et al., 2006). FACS analysis of infected tissues indicated that more CD11b⁺Ly6G⁺ neutrophils were recruited in *Trpv1-Cre/Dta* mice compared to controls (Figure 5C–5D). We observed a similar increase in RTX-treated mice compared to vehicle-treated mice (Figure 5C, 5E). By contrast, we did not detect significant differences in Cd11b⁺Ly6G[−]Ly6C^{hi} monocytes, CD11b⁺Ly6G[−]Ly6C^{lo} monocytes, Cd11b⁺Ly6G[−]Ly6C[−] myeloid cells, or CD11b[−]Cd45⁺ leukocytes (Figure 5D–5E). The host protective effect of RTX-treatment was eliminated by GR1-mediated neutrophil ablation, causing mice to develop dermonecrotic lesions, abscesses, and weight loss similar to controls (Figure S5D–S5F).

TRPV1 neurons release CGRP into infected tissues

Given our observation that *S. pyogenes* induced CGRP release by cultured nociceptor neurons *in vitro* through SLS (Figure 2E), we next determined whether bacterial invasion also induced CGRP release at the infection site using an *ex vivo* organ culture of skin explants (Figure 5F). A significant increase in CGRP levels was observed from biopsies collected 7 h after *S. pyogenes* infection, returning to baseline levels at 24 h (Figure 5G). This CGRP release was TRPV1 neuron dependent, as *Trpv1-Cre/Dta* mice showed reduced CGRP release after *S. pyogenes* infection compared to littermate controls (Figure 5H), and RTX-treated mice showed lower CGRP release in infected tissues compared to vehicle-treated controls (Figure 5H).

BoNT/A dissociates pain perception from neural regulation of host defense

Botulinum neurotoxin A (BoNT/A) is a bacterial toxin that cleaves SNAP-25, a component of the SNARE complex required for neuronal vesicle release (Binz et al., 1994). We used two different protocols of BoNT/A treatment (subcutaneous vs. intrathecal) to dissociate the effects of peripheral neuropeptide release from central pain transmission, to understand the roles of each neuronal process in bacterial infection.

BoNT/A was first injected subcutaneously at the anticipated site of infection 6 days prior to the bacterial inoculum. BoNT/A local treatment dramatically prevented the development of dermonecrotic lesions caused by *S. pyogenes* infection (Figure 6A–6C), with significantly reduced abscess formation (Figure S6A) and body weight loss (Figure 6D). Local BoNT/A treatment had no effect on spontaneous pain and hyperalgesia during infection (Figure S6B–S6C).

By contrast, intrathecal injection of BoNT/A (Figure 6E) efficiently blocked both spontaneous pain and hyperalgesia caused by *S. pyogenes* infection (Figure S6D–S6E), but had no effect on dermonecrotic lesions, abscess size, or body weight loss (Figures 6F–6H, S6F). BoNT/A inhibited *S. pyogenes*-induced CGRP release when applied to cultured DRG neurons (Figure 6I). While subcutaneous BoNT/A treatment inhibited infection-induced CGRP release, intrathecal BoNT/A treatment did not alter this CGRP release (Figure 6J). These results indicate that rather than central pain neurotransmission, peripheral neuropeptide release is likely a key modulator of host defense.

CGRP released by neurons inhibits neutrophil-mediated killing of bacteria

We next asked whether nociceptor neurons could affect the opsonophagocytic killing of *S. pyogenes* by mouse neutrophils. In the presence of cultured nociceptors, the killing of *S. pyogenes* by mouse neutrophils was significantly inhibited (Figure 7A). Pre-treatment of neurons with BoNT/A reversed the suppressive effect of DRG neurons on the capacity of neutrophils to kill *S. pyogenes* (Figure 7A). CGRP receptor antagonists CGRP_{8–37} and BIBN4096, when added to DRG neurons together with neutrophils, each prevented the suppressive effects of DRG neurons on neutrophil killing of *S. pyogenes*. BoNT/A, CGRP_{8–37}, and BIBN4096 did not have direct effects on *S. pyogenes* growth or viability, indicated that they acted on neural-immune signaling (Figure S7A–S7B). We also observed that mouse CGRP inhibited murine neutrophil killing of *S. pyogenes* (Figure 7B), and human CGRP inhibited the killing of *S. pyogenes* by human whole blood (Figure 7C). CGRP inhibited the activity of the bactericidal enzyme myeloperoxidase (MPO) in neutrophil supernatants in a dose-dependent manner in the presence of *S. pyogenes* (Figure S7C).

BoNT/A injection and CGRP receptor antagonism treats infection

We next explored the therapeutic potential of BoNT/A treatment and CGRP receptor antagonism for *S. pyogenes* invasive infection. Local BoNT/A or systemic BIBN4096 treatments, when administered 2 h after infection, were associated with increased bacterial clearance in the skin (Figure S7D), smaller dermonecrotic lesions (Figure 7D) and reduced abscesses compared to mice treated with vehicle alone (Figure S7E). BoNT/A or BIBN4096

increased the recruitment of neutrophils to the infected area compared to infected, untreated mice (Figure S7F).

We next determined if BoNT/A administration at later time points could treat infection. At the 48 h time point, when large lesions were evident, mice were injected with BoNT/A or vehicle at sites around the lesion (Figure 7E). These injections halted the progression of *S. pyogenes* invasion, leading to less dermonecrosis and a rapid decrease in abscess size (Figure 7F–7G). A second BoNT/A injection at day 9 post-infection did not appear to further accelerate resolution of dermonecrotic lesions or abscesses but may have a beneficial effect on weight recovery (Figure S7G).

DISCUSSION

The goals of the present investigation were to determine mechanisms of pain associated with *S. pyogenes* invasion and role of neurons in host defense. We found that pain during infection depended on bacterial production of the toxin SLS. SLS triggered neural release of CGRP into infected tissues, which inhibited neutrophil recruitment and bactericidal activity, facilitating *S. pyogenes* survival. These data indicate that *S. pyogenes* hijacks pain and neural modulation of immunity to drive bacterial invasion. Blocking neuro-immunological signaling using BoNT/A or a CGRP antagonist were identified as strategies to treat infections.

The molecular basis of pain in necrotizing fasciitis

“Pain out of proportion” to physical findings is a hallmark of necrotizing fasciitis. In a survey of clinical parameters, pain was the best predicting factor for distinguishing necrotizing fasciitis from cellulitis (Borschitz et al., 2015). Though pain correlates with disease severity, its underlying mechanisms were unknown. We find that SLS critically mediates pain in mouse models of *S. pyogenes* necrotizing fasciitis. This role was revealed using several strategies: 1) comparison of pain produced by wt and isogenic mutant strains lacking SLS (*sagA*) from two clinical isolates; 2) antibody-mediated neutralization of SLS; and 3) plasmid complementation of SLS in isogenic mutants to restore neuronal activation. SLS-mediated spontaneous pain reflexes in mice maybe analogous to stabbing, sporadic pain experienced by humans during infection. SLS-mediated mechanical hyperalgesia maybe analogous to pressure-induced pain of infected tissues. SLS did not contribute to heat hyperalgesia, a pain modality that requires further investigation.

SLO and SLS are both implicated in *S. pyogenes* evasion of host defenses (Flaherty et al., 2015; Lin et al., 2009; Sierig et al., 2003). SLS is a small oxygen-stable, pore-forming peptide from the thiazole/oxazole-modified microcin family and member of a class of post-translationally modified virulence peptides that occur across several species of pathogenic bacteria (Nizet et al., 2000). SLO, by contrast, is a relatively large oxygen-labile toxin and member of cholesterol-dependent cytolysins (Tweten et al., 2015). We show that SLS, but not SLO, is responsible for the pain of necrotizing fasciitis. We also found that SLS showed more selectivity for TRPV1 neurons at lower bacterial concentrations but activated most DRG neurons at higher concentrations. A recent study showed that SLS activates Band3, an anion exchanger in erythrocytes (Higashi et al., 2015). We do not find Band3 in sensory

neurons in transcriptional datasets (Chiu et al, 2014). Thus, the basis of SLS selectivity for TRPV1 neurons remain unclear.

S. pyogenes infection induced significant nerve loss within the lesion site but not the loss of DRG cell bodies. This finding may relate to necrotizing fasciitis, where intense early pain transitions to local loss of sensation at later time points (Buchanan and Haserick, 1970; Wilson and Haltalin, 1973). The degree of pain and nerve loss is likely a balance between SLS activity and membrane repair. Host cells activate membrane repair processes like microvesicle shedding and lysosomal fusion in response to streptolysins and other PFTs (Romero et al, 2017). Given that SLS is a highly damaging molecule, it may be evolutionarily beneficial for nociceptors to detect SLS and produce pain. Alternatively, *S. pyogenes* could selectively target nociceptors to suppress immunity for its advantage.

Nociceptor neurons suppress immunity and bacterial killing

Neuro-immune interactions at barrier surfaces play a major role in tissue inflammation (Veiga-Fernandes and Mucida, 2016). In the skin, crosstalk between sensory neurons, keratinocytes and immune cells mediate itch in atopic and contact dermatitis (Oetjen et al., 2017; Wilson et al., 2013a, b; Liu et al., 2013). Nociceptors mediate dermal dendritic cell activation in host defense against *C. albicans* (Kashem et al., 2015), and in a mouse model of psoriasis (Gilbert and Ward, 2014; Riol-Blanco et al., 2014). Lung-innervating sensory neurons modulate innate lymphoid cells and T cells to drive allergic airway inflammation (Caceres et al., 2009; Talbot et al., 2015). In the gut, enteroendocrine cells sense bacterial metabolites and signal to sensory neurons (Bellono et al., 2017). Gut-intrinsic enteric neurons and extrinsic sympathetic neurons also crosstalk with muscularis macrophages to regulate gut motility and macrophage tissue-specific programming (Muller et al, 2014; Gabanyi et al., 2016).

Here, we find that nociceptors suppress neutrophil recruitment and function to drive the progression of *S. pyogenes* invasive infection. Neutrophils are the most abundant leukocytes in the blood where they remain in a mature state, poised to migrate towards tissues to control pathogen spread. *S. pyogenes* virulence relies on its capacity to inhibit or resist neutrophils (Okumura and Nizet, 2014). The extent of neutrophil infiltration during human necrotizing fasciitis is variable. A study of biopsies from patients with *S. pyogenes* soft tissue infections showed positive correlation between bacterial load and neutrophil density (Thulin et al., 2006), but surgical exploration in necrotizing fasciitis sometimes revealed thin grayish “dishwater” fluid with few neutrophils despite the presence of large numbers of bacteria (Stevens and Bryant, 2017). *S. pyogenes* produces the proteases ScpC (or SpyCEP) and ScpA to cleave chemotactic factors that mediate neutrophil recruitment, such as CXCL8/IL-8 and C5a. *S. pyogenes* strains lacking expression of these proteases have profoundly attenuated virulence due increased neutrophilic influx (Ji et al., 1996; Kurupati et al., 2010). SLO also silences neutrophil function by damaging phagolysosomal membranes and inducing cell death (Sierig et al., 2003). Our observation that SLS drives pain and neuromodulation of neutrophil killing implies a functional synergism between these toxins in defeating neutrophil function.

Neural suppression of immunity during bacterial invasion may seem counterproductive for host defense. As pain accompanies inflammation, it is possible that neuromodulation of immunity evolved as a feedback mechanism to limit injury from excessive inflammation. In the case of *S. pyogenes* infection, SLS hijacks this neuroimmune communication by stimulating neuropeptide release and consequently blocking host defense.

A potential strategy to treat *S. pyogenes* invasion and necrotizing fasciitis

Necrotizing fasciitis is a life-threatening condition in which treatment with surgical debridement, antibiotic therapy, and intensive supportive care have only limited efficacy, and mortality remains unacceptably high. Our work identifies three approaches as potential therapies: 1) Neutralizing SLS with a specific antibody, 2) BoNT/A to inhibit CGRP release, and 3) BIBN4096 to inhibit CGRP receptor signaling. BoNT/A is currently used in cosmetic dermatology and treatment of migraine (Grando and Zachary, 2017). Neutralizing anti-CGRP antibodies and CGRP receptor antagonists are also being developed for migraine (Petersen et al., 2005; Tso and Goadsby, 2017).

BoNT/A has been shown previously to act on nociceptors to block pain transmission (reviewed in Matak and Lackovi , 2014). We now find that BoNT/A can also block neuronal suppression of the local immune response, unrelated to pain perception. It is important to note that BoNT/A could also act on other cell-types including skin-innervating cholinergic and sympathetic neurons (Grando and Zachary, 2017), that may in turn modulate immune function (Chavan et al., 2017). BoNT/A may also target epithelial cells and skin immune cells (Grando and Zachary, 2017).

CGRP could similarly mediate functions in *S. pyogenes* infection beyond suppression of neutrophil function. In the skin, the CGRP receptor complex (Ramp1/Calcrl) is expressed by vascular endothelial cells, smooth muscle cells, keratinocytes, fibroblasts, and some immune cells (Granstein et al., 2015; Pinho-Ribeiro et al., 2017). CGRP acts on vascular cells to induce vasodilation, mediates keratinocyte proliferation to accelerate wound healing, and modulates Langerhans cells and dermal dendritic cells to polarize Th2 responses. It remains to be determined whether these other cell-types contribute to neural suppression of host defense.

We found that BoNT/A injections after the development of dermonecrosis blunted the progression of *S. pyogenes* invasion in mice. There are important differences in *S. pyogenes* pathogenesis between mouse and human (Olsen and Musser, 2010), as humans are the only natural hosts of *S. pyogenes*. Despite this limitation, mouse models of soft tissue infection have been utilized to demonstrate the role of major virulence determinants such as surface M protein and the hyaluronic acid capsular polysaccharide (Ashbaugh et al, 1998; Schrager et al., 1996). Of particular relevance to our work, soft tissue infection models in mice support a role in virulence for SLS (Betschel et al., 1998; Datta et al., 2005). SLS also mediates infection of human oropharyngeal keratinocytes and macrophages (Bastiat-Sempe et al., 2014; O'Seaghdha and Wessels, 2013). Future studies beyond murine models are needed to investigate the translational potential of our findings in enhancing host immunity against bacterial invasion.

In conclusion, neurons and their signaling to the immune system have a major impact on the outcome of bacterial soft tissue infection. BoNT/A and CGRP antagonists may be repurposed for treatment of infections due to *S. pyogenes* and perhaps other bacterial pathogens. Targeting the peripheral nervous system could provide therapeutic approaches in invasive infections including necrotizing fasciitis.

STAR METHODS

CONTACT FOR REAGENT AND RESOURCE SHARING

All unique reagents and resources will be made readily available upon request to the Lead Contact, Dr. Isaac Chiu (isaac_chiu@hms.harvard.edu).

EXPERIMENTAL MODEL AND SUBJECT DETAIL

Human blood donors—Blood samples were collected by a trained phlebotomist from three healthy adult volunteers of either sex at Boston Children’s Hospital with approval from the hospital’s Institutional Review Board (protocol X04-01-008). Written informed consent was obtained from all volunteers. No further demographic data was collected from the volunteers. Blood collected was from a single donor per experiment and was not pooled.

Animals—All animal experiments were approved by the Institutional Animal Care and Use Committee (IACUC) at Harvard Medical School and were conducted in accordance with National Institutes of Health (NIH) animal research guidelines. C57BL6/J, B6(Cg)-*Rag2^{tm1.1Cgn}*/J, B6N.129S2-*Casp1^{tm1Flv}*/J, B6.129P2(SJL)-*Myd88^{tm1.1Defr}*/J, B6.129-*Trpv1^{tm1(cre)Bbm}*/J, B6.129P2-*Gt(ROSA)26Sor^{tm1(DTA)Lky}*/J, and B6.129X1-*Trpv1^{tm1Jul}*/J mice were purchased from Jackson Laboratories (Bar Harbor, ME). Mice were bred and housed in individually ventilated micro isolator cages within a full barrier, specific pathogen-free animal facility at Harvard Medical School under a 12 h light/dark cycle with ad libitum access to food and water. B6.129-*Trpv1^{tm1(cre)Bbm}*/J heterozygous (+/-) mice were bred with B6.129P2-*Gt(ROSA)26Sor^{tm1(DTA)Lky}*/J homozygous (++) mice to generate nociceptor-ablated *Trpv1-Cre/Dta* (*Trpv1-Cre^{+/-}/Dta^{+/-}*) mice and control littermates (*Trpv1-Cre^{-/-}/Dta^{+/-}*). Both male and female age-matched mice from 6 to 14 weeks of age were used for all experiments in this study. Male and female mice were similarly susceptible to *Streptococcus pyogenes* infection. Individual animal health status was routinely monitored by Harvard Center for Comparative Medicine veterinary staff. Additionally, one cage containing two sentinel animals was maintained on each rack. These sentinel cages were supplied with pooled samples of soiled bedding from regular colony animals at every cage change. All cage changes were performed in Class II biosafety change stations. Animal sentinels were tested quarterly for pinworms, fur mites, Sendai virus, Pneumonia virus of mice, Mouse hepatitis virus, GD-7 virus, Minute virus of mice, Mycoplasma pulmonis, Mouse parvovirus, Epizootic diarrhea of infant mice, Reo-3 virus, and annually for ectromelia virus and lymphocytic choriomeningitis virus. Only healthy animals were used for experiments. Euthanasia was performed by CO₂ inhalation.

Bacterial strains and culture—All procedures related to bacterial strains and infectious disease work were approved by the Committee on Microbiological Safety (COMS) at

Harvard medical school and were conducted under Biosafety Level 2 protocols and guidelines. All *Streptococcus pyogenes* strains used in this study are listed in the Key Resources Table. *S. pyogenes* 854 M-type 1 was originally isolated from a patient with retroperitoneal abscess (Gryllos et al, 2008). *S. pyogenes* 950771 M3 serotype strain is a clinical isolate obtained from a patient with necrotizing fasciitis and sepsis (Ashbaugh et al, 1998). These founder bacterial strains were mutated to generate isogenic mutant strains (see Methods Details). Bacteria were grown on Tryptic Soy Agar (TSA) plates supplemented with 5% Sheep Blood (BD Biosciences, Cat# 221239), or grown in liquid culture in Todd-Hewitt Broth (Sigma, Cat# T1438) supplemented with 0.2% yeast extract (Sigma, Cat# Y1625) (THY broth) at 37°C with 5% CO₂. When required, THY broth was supplemented with spectinomycin (50 µg/mL, Sigma, Cat# S4014). For storage, bacterial glycerol frozen stocks (20% glycerol, Sigma, Cat# G5516) of *S. pyogenes* strains were prepared and kept at -80°C until use.

Primary cells culture—Murine DRG neurons were obtained from healthy naïve animals as described in *Dorsal root ganglia neuron dissection and culture*. Mouse neutrophils were isolated from mouse bone marrow as described in *Neutrophil isolation and killing assays*.

DRG neurons were maintained under sterile conditions in a humidified incubator at 37°C and 5% CO₂. For calcium imaging experiments, DRG neurons were incubated for 12–24h in 35 mm laminin (20 µg/mL, Thermo Fisher, Cat# 23017015)-coated sterile cell culture dishes (VWR International, Cat# 10062-888) containing 2 mL of neurobasal-A medium (Thermo Fisher, Cat# 21103049), B-27 supplement (Thermo Fisher, Cat# 1704044), penicillin/streptomycin (100 units/mL and 100 µg/mL, Thermo Fisher, Cat# 15140122), L-glutamine (2 mM, Thermo Fisher, Cat# 25030081) and mouse NGF (50 ng/mL, Thermo Fisher, Cat# 50385MNAC50).

For the experiments involving *in vitro* CGRP release assays by neurons, or co-incubation of DRG neurons with neutrophils, DRG neurons were first incubated for one week in laminin (20 µg/mL, Thermo Fisher, Cat# 23017015)-coated sterile flat bottom 96-wells plates (Thermo Fisher, Cat# 08-772-53) containing 200 µL of neurobasal-A medium (Thermo Fisher, Cat# 21103049), B-27 supplement (Thermo Fisher, Cat# 1704044), penicillin/streptomycin (100 units/mL and 100 µg/mL, Thermo Fisher, Cat# 15140122), L-glutamine (2 mM, Thermo Fisher, Cat# 25030081), mouse NGF (50 ng/mL, Thermo Fisher, Cat# 50385MNAC50), and cytosine arabinoside (10 µM, Sigma, Cat# C6645). Half of the medium was replaced with fresh media every two days. At day 7, neurons were stimulated for CGRP assays or co-cultured with neutrophils for experiments as described in *Neuronal stimulation and CGRP release* and in *Neutrophil isolation and killing assays* sections.

Skin biopsies—Skin punch biopsies were collected as described in the section “*CGRP release assay from skin explants*” from the flank area injected with vehicle or bacteria. Samples were collected under sterile conditions, rapidly transferred to sterile 24-well cell culture plates (Genesee Scientific, Cat# 25-107) containing 1 mL of DMEM (Thermo Fisher, Cat# 11995073) at 32°C and immediately used for experiments.

METHOD DETAILS

Generation of isogenic mutant *S. pyogenes* strains—The *slo*-negative derivatives of the *S. pyogenes* 854 and 950771 were generated by allelic exchange as described previously (Love et al., 2012; Bricker et al., 2002). Genomic DNA for use as a PCR template was prepared from an overnight culture of *S. pyogenes* as follows: Cells from a 10 mL overnight culture were harvested by centrifugation at 10,000 rpm and resuspended in 1 mL of STE buffer (100 mM NaCl, 10 mM EDTA, 10 mM Tris, pH 8.0) containing mutanolysin (50 µg, Sigma). This suspension was incubated at 37°C with agitation for 2 h at which point DNase-free RNase (10 µg; Sigma) and *N*-Lauroylsarcosine (0.5% (v/v), Sigma) were added. After a further 10 min incubation at 37°C, pronase was added (10 mg, Sigma) and the mixture was incubated at 37°C for a further 10 min. *S. pyogenes* genomic DNA was precipitated by mixing with an equal volume of phenol:chloroform (1:1), followed by centrifugation at 12,000 rpm. The pellet was washed with ice-cold ethanol and then washed and dissolved in TE buffer (10 mM Tris, pH 8.0, 1 mM EDTA). For PCR, 1 µL of genomic DNA template in a 50 µL PCR reaction mixture was used. PCR products corresponding to the 5' and 3' ends of *slo* were produced using the primer pairs 5' - CCCTCTAGAGGTAACCTTGTTACTGCTAATGC-3' and 5' - CCCGGATCCCAGTGACAGAGTCAATGATGG-3' (441 bp product) and 5' - CCCGAATTCGCGGGTGTCAATAACAGAACTG-3' and 5' - CCCGGTACCCCATATGGGCTCAGGGTTGATC-3' (367 bp product), respectively. All PCR reactions were performed using Phusion High-Fidelity PCR Master Mix (New England Biolabs). The products were directionally cloned into the temperature-sensitive shuttle vector pJRS233 (provided by June Scott) (Perez-Casal et al., 1993) using unique *Xba*I, *Bam*HI, *Eco*RI and *Asp*718 restriction endonuclease sites (underlined) incorporated into the PCR primers. The final construct representing the *slo* sequence with an 818 bp internal deletion was cloned into pJRS233 at the *Xba*I and *Asp*718 sites. The resultant plasmid, p*J*slo was verified by DNA sequencing (Genewiz) using the primers pJRSseqF (5'-GGGATGTGCTGCAAGGCG-3') and pJRSseqR (5'-ACGACAGGTTTCCCGACTG-3'), which recognize regions outside the 5' and 3' termini of the pJRS233 multiple cloning site.

The p*J*slo plasmid was introduced into competent *E. coli* DH5α cells (New England Biolabs) by transformation according to the manufacturer's instructions. This plasmid was purified using the Plasmid midi- or maxi-prep kits (Qiagen) and transformed into electrocompetent *S. pyogenes* cells. Plasmid integration followed by allelic exchange was allowed to occur at the permissive temperature (Perez-Casal et al., 1993). Mutants were verified by PCR of the *slo* gene using the first and forth primers listed above and Phusion® High-Fidelity PCR Master Mix (New England Biolabs).

SLS was inactivated in *S. pyogenes* 854 and 950771 by deletion of *sagA* (Sierig et al., 2003). DNA fragments corresponding to regions at the 5' (359 bp) and 3' (392 bp) termini of *sagA* were generated using the primer pairs 5' - CGCGGATCCCACATAGTTATTGATAGAAT-3' and 5' - TCCAGGAGCAACTTGAGTTG-3' (5') and 5' - CAACTCAAGTTGCTCCTGGACAAGGTGGTAGCGGAAGTTA-3' and 5' - GCGAAGCTTGTAATCCGATAAGGACAAGT-3' (3'). These fragments have overlapping

ends at the 3' and 5' ends, respectively to permit a subsequent overlap PCR, using the first and fourth primers listed above. The resultant PCR product harbored an internal 60-bp deletion in *sagA*. This product was directionally cloned into pJRS233 using the unique *Bam*HI and *Hind*III restriction endonuclease sites included in the PCR primers (underlined), to generate pJ*sagA* in *E. coli* strain DH5 α . Plasmid pJ*sagA* was purified and used to generate 950771 *sagA* and 854 *sagA* as described above for *slo*. Mutants were identified by their lack of beta hemolysis on blood agar and verified by PCR analysis of the *sagA* locus. To generate *slo sagA* mutants, pJ*sagA* was introduced to 950771 *slo* or 854 *slo* by allelic replacement as described above.

For complementation studies, the *sagA* gene including a 780 bp promoter region upstream (Nizet et al., 2000) was cloned using the primer pair 5'-CCGGAATTCGGCCCAAGAACGGAGTGTAT-3' and 5'-GGAGCATGCTTATTACCTGGCGTATAACTTCCG-3'. This product was directionally cloned using *Eco*RI and *Sph*I (underlined in primer sequence) into pDL278, to generate pSagA. Plasmid pSagA was purified and introduced into *sagA* and *slo sagA* backgrounds by electroporation and maintained by selection using spectinomycin (Sigma). Positive transformants were verified by PCR and their restoration of beta hemolysis on blood agar medium.

Streptolysin O activity—SLO activity was measured by determination of hemolytic titers of bacterial supernatants of *S. pyogenes* taken at early stationary phase. Supernatants were filtered through a 0.45 mm membrane, Dithiothreitol added at 6 mM and incubated at 37°C for 30 min. Sheep erythrocytes was prepared by diluting fresh defibrinated sheep blood (Northeast Lab Services) in PBS and the suspension was added to each bacterial culture sample. After 30 min incubation at 37°C, cell mixtures were centrifuged, and absorbance measured at 550 nm. Hemolytic units correspond to the reciprocal of the dilution of supernatant that yielded 50% lysis, where 100% lysis corresponds to that caused by 1% Triton X-100. Hemolytic activities were also determined after pre-treatment of samples with the SLO inhibitor, cholesterol (cholesterol-methyl- β -cyclodextrin, Sigma) at a concentration of 250 μ g/mL (estimated cholesterol concentration, 10 μ g/mL).

General experimental design—All *in vivo* experiments were performed in both male and female age-matched littermates. Pain behavioral tests were performed by blinded observers that were unaware of treatment groups and genotypes. Treatment groups of mice were randomized and evenly distributed across both male and female littermates in cages. Treatments were performed by blinded investigators unaware of the contents of syringes or other administration devices. In experiments involving transgenic mice, littermates with different genotypes were cohoused for the duration of experiments. Quantification and analysis of microscopy images were performed by a blinded investigator unaware of groups and genotypes.

Animal numbers for pain behavioral analysis and infection outcome measurements were estimated based on pilot studies of *S. pyogenes* infections in our lab and based on standard numbers used in the field based on publications on pain and bacterial infection work. For pain behavioral tests, we used at least 4 mice per group. For lesion size and pain behavioral

experiments, mice that did not survive the entire time-course of analysis were excluded from analysis. For bacterial infections and analysis (demonecrotic lesion size, abscess size, and weight loss following infection), we used at least 5 mice per group. For histology, bacterial load recovery analysis, flow cytometry, *ex vivo*, and *in vitro* experiments, we used at least 3 biological replicates per group. All statistical analysis was performed using Graphpad Prism (v. 7.02). For specific numbers of replicates used for each experiment, please see the section *Quantification and Statistical Analysis*.

Bacterial infections—*S. pyogenes* strains were grown overnight on TSA plates supplemented with 5% Sheep Blood (BD Biosciences, Cat# 221239) at 37°C with 5% CO₂. The next morning, bacterial colonies were picked and inoculated into THY broth (Todd-Hewitt Broth, Sigma, Cat# T1438, with 0.2% yeast extract, Sigma, Cat# Y1625), incubated for 3 h at 37°C without shaking until growth reached mid-exponential phase, and resuspended in fresh medium to A_{600nm} of 0.6. Bacterial cells were collected by centrifugation at 800g for 15 min, washed once in PBS, and then resuspended in PBS at different estimated concentrations for injection. Before injection of bacteria, mice were lightly anesthetized by inhalation of isoflurane (Patterson Veterinary) 3% in oxygen using a precision vaporizer. For hind paw infections, a single dose of 5×10⁵ – 5×10⁸ cfu of *S. pyogenes* in 20 μL PBS was administered by intraplantar injection of the right hind paw using a 0.5 cc syringe fitted with a 31-gauge needle (BD Biosciences). For flank infections, 5×10⁶ cfu of *S. pyogenes* in 50 μL PBS was injected subcutaneously into the flank previously shaved using a hair clipper (Patterson Veterinary). In some cases, hair removal cream (Nair) was also applied for hair removal prior to infection. The bacterial suspension was kept on ice until use, and the inoculum was confirmed by quantitative culture of an aliquot of the final suspension prior to injection. Injections of bacteria or vehicle were performed by an investigator blinded to the content of syringes. Syringes were previously assigned to specific animals by an investigator aware of the groups in order to distribute groups across multiple cages.

Bacterial load recovery analysis—Mice were euthanized by CO₂ inhalation and rapidly used for tissue dissection. During necropsy of mice, total hind paw tissues including epidermis, dermis, and subcutaneous tissue to the tendons, or flank tissue encompassing the injection site including epidermis, dermis, and subcutaneous tissue, or spleens were dissected and weighed. Tissues were then transferred to 2 mL eppendorf tubes containing 5 mm stainless steel beads (Qiagen, Cat# 69989) and 1 mL of ice-cold sterile distilled water. Tissues were homogenized using a TissueLyser II (Qiagen) for 10 min at 30 Hz. To determine bacterial load recovery, serial dilutions were made and plated on TSA plates with 5% Sheep Blood plates (BD Biosciences, Cat# 221239), and colonies were counted after overnight incubation at 37°C with 5% CO₂.

Pain behavioral tests—Spontaneous pain behaviors were evaluated by quantifying the time that mice spent 1) lifting/licking the hind paw and 2) the number of paw flinches that occurred over a 1 h time period immediately after infection. Data was collected in 5-minute intervals. For mechanical and heat hyperalgesia tests, mice were allowed to habituate to the apparatus during 2 h and for three consecutive days before the beginning of measurements.

After habituation, baseline measurements were obtained on two consecutive days prior to infection. Pain intensity to mechanical stimulus (mechanical hyperalgesia) was measured using von Frey monofilaments. Briefly, mice were placed on an elevated wire framework and a series of von Frey monofilaments with different pressure intensities (from 0.007 g to 4 g) were applied to the plantar surface of the infected hind paw. The threshold of pain was determined as the lowest pressure filament that induced a response (paw withdrawal) in five out of ten applications. To measure pain sensitivity to a heat stimulus (heat hyperalgesia), mice were placed on the temperature-controlled (29°C) glass plate of a Hargreaves apparatus (Model 390G, IITC Life Science). A radiant heat source (active intensity 23%) was used to stimulate the infected paw by gradually increasing the temperature of the plantar surface. The threshold of pain was determined as the latency (in seconds) to evoke a response of paw withdrawal. The mean of three measurements was determined for each animal at each time point. An exposure limit of 40 s was used to prevent tissue damage. Data from mice that did not survive until the end of the tests were not included in the analysis. Pain behavior tests were performed by blinded observers that were unaware of the treatments, groups, and genotypes.

Lesion size measurement—One day prior to subcutaneous injection with *S. pyogenes*, mice were lightly anesthetized by inhalation of isoflurane (Patterson Veterinary) 3% in oxygen using a precision vaporizer, and the flank area was shaved using a hair clipper. Abscess sizes and dermonecrotic skin lesions were measured daily with a digital caliper (VWR International, Cat# 62379-531) for 14 days after injection, and area calculated with the formula $A=(\pi/2)(\text{length})(\text{width})$. Mice were also anesthetized with isoflurane 3% in oxygen during the measurements. Data from mice that did not survive until the end of the tests were not included in the analysis.

In vivo BoNT/A and BIBN4096 treatments—Botulinum neurotoxin A (BoNT/A, List Biological Labs, Cat# 130B) intrathecal or local subcutaneous pre-treatments were used that were able to distinguish the contribution of pain perception from peripheral neuropeptide release. Mice were subsequently infected with M1 *S. pyogenes* in the footpad for pain behavioral assays or in the flank for dermonecrotic lesion measurements. For intrathecal pre-treatments, BoNT/A (25 pg in 5 μ L PBS) or vehicle (5 μ L PBS) was injected at the level of L4–L6 segments of spinal cord 24 h before infection with *S. pyogenes*. For local pre-treatments, different groups of mice received a subcutaneous BoNT/A injection (25 pg in 5 μ L PBS) or vehicle (5 μ L PBS) in the footpad, or they received BoNT/A (25 pg in 100 μ L PBS) or vehicle (100 μ L PBS) in the for flank skin at the anticipated site of infection 6 days before infection. We also evaluated whether BoNT/A or CGRP antagonist (BIBN4096, Tocris, Cat# 4561) was able to treat *S. pyogenes* infection. For these experiments, mice were infected in the flank skin with *S. pyogenes* M1. 2 h after infection, we performed subcutaneous injection of BoNT/A (25 pg in 50 μ L PBS) at the site of infection or intraperitoneal injection of CGRP receptor antagonist BIBN4096 (30 mg/kg). In another set of experiments to determine therapeutic potential, BoNT/A or vehicle was administered locally in mice infected with *S. pyogenes* at day 2 after flank skin infection, and again at day 9 after infection. For this experiment, BoNT/A (25 pg in 100 μ L PBS) or vehicle (100 μ L PBS) was distributed in 5 applications of 20 μ L each around the borders of the lesion at day

2 and at day 9. The injection sites were marked using a blue marker at each day of injection. BoNT/A was administered using a Hamilton syringe (Hamilton Company, Cat# 7636-01) fitted with a 32 gauge needle (Hamilton Company, Cat# 7803-04). *S. pyogenes* M1 wt was used at the following doses for the experiments described above: 5×10^6 cfu for flank infections and lesion size measurements, 5×10^7 cfu for foot pad infections and hyperalgesia studies, and 5×10^8 cfu for foot pad infections and spontaneous lifting/licking/flinching tests.

Histology—Mice were euthanized by CO₂ inhalation and intracardially perfused with 30 mL of ice-cold PBS, followed by 30 mL of PBS/4% paraformaldehyde (PFA, Sigma, Cat# P6148). Infected hind paw and flank lesion samples were dissected, post-fixed for 12 h at 4°C in PBS/4% paraformaldehyde solution, embedded in paraffin, sectioned, and stained using hematoxylin and eosin (H&E) or Brown and Brenn Gram stains by the Harvard Medical School Rodent Histopathology Core. Stained sections were imaged by light microscopy on an Eclipse Ti-S/L100 inverted microscope (Nikon), and images collected by NIS-Elements AR software.

Immunostaining and microscopy—For immunofluorescence staining, hind paw skin tissues and dorsal root ganglion (DRG) tissues were dissected from mice previously euthanized by CO₂ inhalation and intracardially perfused with 30 mL of PBS, followed by 30 mL of PBS/4% PFA (Sigma, Cat# P6148). Samples were post-fixed in PBS/4% PFA solution at 4°C for 12 h, cryoprotected in PBS/30% sucrose (Sigma, Cat# S0389) for 3 days at 4°C, embedded in Optimal Cutting Temperature (OCT, Sakura Finetek, Cat# 4583), and stored at -80°C until processing. Cryosections (20 µm for DRG, 40 µm for skin) were cut onto Superfrost Plus slides (Thermo Fisher) before immunostaining. Hind paw skin or DRG sections were stained with mouse or rabbit anti-beta III tubulin (Tuj1, Abcam, 1:500), rabbit anti-CGRP (Sigma, 1:10,000), mouse anti-NF200 (MilliporeSigma, 1:1000), mouse anti-PGP9.5 (Abcam, 1:500), or guinea pig anti-TRPV1 (MilliporeSigma, 1:1000), followed by Alexa 594 donkey anti-mouse IgG (Abcam, 1:500), DyLight 488 donkey anti-rabbit IgG (Abcam, 1:500) or goat anti-guinea pig IgG (Sigma, 1:500). Stained sections were mounted in Vectashield mounting medium (Vector Labs, Cat# H1000), with addition of DAPI (BioLegend, Cat# 422801) for skin samples. Fluorescence imaging was performed using a FV1000 laser-scanning confocal microscope (Olympus). Data were collected using Olympus Fluoview software. Samples were imaged with z-stacks of 1 µm steps and 20 µm (for DRG) or 40 µm (for skin) total thickness; maximum projection images were exported for analysis.

Quantification of DRG neurons—DRG samples were collected, sectioned, stained, and imaged as described in the section *Immunostaining and microscopy*. Maximum projection images (3 fields per sample) obtained for each channel were exported for analysis. The number of TRPV1, CGRP, or NF200 positive neurons, and the total number of neurons (βIII-tubulin positive) field were quantified by an investigator blinded for the groups. Percentage of TRPV1, CGRP, or NF200 positive neurons out of the total neurons (βIII-tubulin positive) was determined for each sample as the average of 3 fields.

RTX mediated ablation of nociceptor neurons—Resiniferatoxin (RTX, Sigma-Aldrich), a potent capsaicin analog, was used to deplete TRPV1-positive nociceptors. Male

and female 4-week-old C57BL/6 mice were lightly anesthetized by inhalation of isoflurane (Patterson Veterinary) 3% in oxygen using a precision vaporizer. Three RTX escalating doses (30 µg/kg, 70 µg/kg, 100 µg/kg, diluted in PBS with 1.2% DMSO and 0.06% Tween-80) were subcutaneously injected over the flank of anesthetized mice on three consecutive days, as adapted from established protocols (Riol-Blanco et al., 2014). Control littermates were injected with vehicle solution on the same days (PBS with 1.2% DMSO and 0.06% Tween-80). Mice were used for infection experiments four weeks after the last injection of RTX. Vehicle and RTX treated mice were housed together before and during the experiments. Efficiency of RTX treatment in depleting TRPV1-positive nociceptors was confirmed by counting the number of TRPV1-positive neurons in the DRG by microscopy. DRG samples were collected, sectioned, and stained as described in the section *Immunostaining and microscopy*, and quantified as described in the section *Quantification of DRG neurons*.

Dorsal root ganglia neuron dissection and culture—Adult, 7 – 13 wk old male and female mice were euthanized by CO₂ inhalation. Dorsal root ganglia (DRG) were dissected from all segments of the spinal cord and transferred to neurobasal medium (Thermo Fisher) supplemented with B-27 (Thermo Fisher) and penicillin/streptomycin (Thermo Fisher). DRGs were enzymatically dissociated by incubating in 2 mL of HEPES-buffered saline (Sigma) containing collagenase A (1 mg/kg, Sigma) and dispase II (2.4 U/mL, Roche Applied Sciences) for 20 min at 37°C. Supernatant was carefully removed, replaced with 2 mL of fresh collagenase A/dispase II solution and incubated for 20 min at 37°C again. Cells were transferred to a tube containing 10 mL of DMEM/10% FBS (Thermo Fisher), centrifuged for 1 min at 200g at 4°C, and resuspended in 800 µL of DMEM/10% FBS containing DNase I (150U/mL, Thermo Fisher). DRG cells were dissociated with fire-polished glass Pasteur pipettes (VWR International) with decreasing tip diameters to create single-cell suspensions. Cells were resuspended in 2 mL of neurobasal medium (Life Technologies), and then centrifuged (260g, 10 min) after overlaying on a 10% bovine serum albumin (BSA) gradient (diluted in Neurobasal medium from a 30% BSA solution in PBS, Sigma). Supernatant was removed and resulting pellet resuspended in neurobasal medium for plating. For calcium imaging, cells were plated onto 35 mm laminin-coated (Thermo Fisher) cell culture dishes (2,000 cells per dish) in neurobasal-A medium plus 50 ng/mL nerve growth factor (Thermo Fisher); DRG neurons were used for calcium imaging 12 – 24 h after plating. For co-incubation with neutrophils and CGRP release experiments, 5,000 DRG neurons were seeded per well in laminin-coated flat bottom 96-wells plates and incubated with neurobasal-A medium plus 50 ng/mL nerve growth factor (Thermo Fisher) and cytosine arabinoside (10 µM, Sigma) for one week; half of the medium was replaced with fresh media every two days.

Calcium imaging and data analysis—Cultured DRG neurons were washed and loaded with 5 µM Fura-2 AM (Thermo Fisher) in Neurobasal-A medium for 30 min at 37°C, then washed twice and imaged in Krebs-Ringer solution (Boston BioProducts). DRG neurons were imaged using an Eclipse Ti-S/L100 inverted microscope (Nikon) and Zyla sCMOS camera (Andor). An ultraviolet light source (Lambda XL lamp, Sutter Instrument) was used for excitation of Fura-2-AM by alternating 340 nm and 380 nm wavelengths. NIS-elements

software (Nikon) was used to image, process and analyze 340/380 ratiometric images from neurons. An increase in 340/380 ratio of 10% or more from baseline levels was considered a positive response to a ligand. For calcium imaging experiments, cell size for individual DRG neurons (measured as area in μm^2) was determined using NIS-elements software by marking individual cells using the Region of Interest tool in combination with the Automated Measurement tool (Nikon). The percentage of bacteria-responsive cells or bacteria-unresponsive cells from 3 separate neuronal fields/condition was determined and binned into four groups for analysis based on their cell body area (<149, 150–249, 250–349, and >350 μm^2).

S. pyogenes supernatant for neuronal stimulation—*S. pyogenes* strains were grown overnight on TSA plates with 5% sheep blood (BD Biosciences) at 37°C in 5% CO₂. Bacterial colonies were picked and inoculated into liquid cultures of THY broth, grown for 3 h at 37°C without shaking until mid-exponential phase, and bacterial density estimated by A_{600nm}. Bacterial cells were collected by centrifugation, washed, and then resuspended (5×10^8 – 5×10^{10} cfu per mL) in phenol red-free neurobasal-A medium plus 6% BSA (Sigma) and incubated at 37°C for 1 h, centrifuged for 15 min at 800g, and the supernatant filtered with a 20 μm cell strainer. For calcium imaging, DRG neurons were stimulated with 200 μL of the filtrate, representing bacterial supernatant. For CGRP release assay, 50 μL of bacterial supernatant was used.

Neuronal stimulation and CGRP release—DRG neurons (5,000 per well) were cultured for one week in Neurobasal-A medium containing 50 ng/mL nerve growth factor and cytosine arabinoside as described in the sections *Dorsal root ganglia neuron dissection and culture*. One group of neurons was treated with 25 pg (in 200 μL of Neurobasal-A medium) of Botulinum neurotoxin A (BoNT/A) for 24 h prior to neuronal stimulation. The neuronal culture medium was removed from all wells, and 200 μL of fresh neurobasal-A medium was added to the wells. Filtered supernatants from *S. pyogenes* M1 854 strain or isogenic mutant strains were collected at the day of the test as described in the section *S. pyogenes supernatant for neuronal stimulation*. Immediately before stimulation, 50 μL of cell culture supernatant was removed and 50 μL of bacterial supernatant or control medium (neurobasal-A medium + 6% BSA) was added to the wells. Cells were incubated for 30 min at 37°C and with 5% of CO₂ and then 50 μL of supernatant were collected to determine CGRP concentration. A CGRP Enzyme Linked Immunosorbent kit (Cayman Chemical) was used to quantify CGRP according to manufacturer's instructions.

Neutrophil isolation and killing assays—Following euthanasia, femurs and tibias were dissected from mice. Bone marrow cells were flushed out using PBS/1 mM EDTA (Sigma) in a syringe and a 21 gauge needle. Cells were then strained through a 100 μm cell strainer, centrifuged for 5 min at 300g, resuspended in 3 mL of red blood cell lysis buffer (eBioscience) and incubated for 15 min at room temperature. PBS (22 mL) was added and the cells were centrifuged for 5 min at 300g. Supernatant was removed, and the cells were resuspended in neurobasal-A medium (Thermo Fisher) with 10% fetal bovine serum (FBS) at a maximum concentration of 1×10^8 cells/mL. Neutrophils were isolated using an immune magnetic negative selection kit according to manufacturer's instructions (EasySep mouse

neutrophil enrichment kit and EasySep Magnet, StemCell). Half of the final neutrophil suspension solution was saved to collect the supernatant. This supernatant was added to the conditions where neutrophils were absent (control conditions) instead of fresh media to control for effects of used cell media on bacterial growth.

For opsonophagocytic killing assays, mouse neutrophils were used immediately after isolation. *S. pyogenes* (5×10^3 cfu) M1 wt strain was mixed with mouse neutrophils (5×10^5 cells per well) in 200 μ L of neurobasal-A medium containing 10% of fresh mouse serum. As described before, neutrophil filtered supernatant was added to the control conditions (without neutrophils). CGRP (1 μ M, GenScript) or the antagonists CGRP₈₋₃₇ (1 μ M, GenScript) or BIBN4096 (1 μ M, Tocris) were added to the cultures immediately before *S. pyogenes*. For neuron-neutrophil co-incubation experiments, neutrophils and bacteria were added to the plates containing 5×10^3 DRG neurons and incubated under the same conditions. One group of DRG neurons was treated with 25 pg (200 μ L) of BoNT/A 24 h before the assay. Some wells of neuron-neutrophil co-cultures were treated with the antagonists CGRP₈₋₃₇ (1 μ M, GenScript) or BIBN4096 (1 μ M, Tocris) at the time of neutrophil addition.

For all conditions described for neutrophil opsonophagocytic killing assays, plates were incubated for 1h at 37°C with gently shaking (150 rpm). The amount of extracellular and intracellular bacteria was determined after resuspension in ice-cold ddH₂O by serial dilution plating on TSA plates with sheep blood agar (BD Biosciences), and bacterial colonies were counted after overnight incubation at 37°C in 5% CO₂. The multiplication factor of net bacterial growth was calculated as the number of cfu recovered/ number of cfu added to wells.

Neutrophil myeloperoxidase activity (MPO) assay—Mouse neutrophils were isolated from mouse bone marrow using EasySep mouse neutrophil enrichment kit and EasySep Magnet according to manufacturer's instructions (StemCell). These neutrophils (5×10^5 cells per well) were then treated with CGRP (0.01–1 μ M, GenScript) or vehicle (PBS), immediately prior to mixture with *S. pyogenes* (5×10^3 cfu) M1 wt strain or vehicle (PBS) in 200 μ L of neurobasal-A medium containing 10% of fresh mouse serum. Serum was obtained after coagulation of whole mouse blood. Plates were incubated for 30 min at 37°C with gently shaking (150 rpm), and supernatant collected for MPO activity measurements. Supernatants (50 μ L) were added to 200 μ L of 50 mM phosphate buffer solution (pH 6.0) containing 0.167 mg/mL of peroxidase substrate *o*-dianisidine dihydrochloride (Santa Cruz Biotech) and 0.05% hydrogen peroxide (Santa Cruz Biotech) and incubated for 30 min at room temperature. MPO activity was determined spectrophotometrically by measuring the increase in absorbance at 450 nm.

Lancefield assay—Human blood phagocytosis assays (Lancefield bactericidal test) were performed as described previously with slight modifications (Gryllos et al., 2008). *S. pyogenes* M1 wt strain was cultured to OD₆₀₀ of 0.15 in L3 medium at 37°C with 5% CO₂ and diluted in sterile PBS. Quantitative cultures of the bacterial suspension were performed to allow precise quantification of the starting inoculum. Whole human blood (10 mL/tube) was collected into heparin-containing tubes (BD Vacutainer™, Fisher Scientific)

Approximately 20–200 *S. pyogenes* cfu were inoculated into heparinized whole blood obtained from three healthy donors supplemented with human CGRP (10 or 100 nM) and incubated for 3 h at 37°C with end-over-end rotation. Bacterial survival was quantified as multiplication factor of number of surviving colonies relative to the starting inoculum. Each condition was tested in triplicate.

CGRP release assay from skin explants—Skin punch biopsies (12 mm) were collected from the uninfected or infected flank skin samples of euthanized mice, and rapidly transferred to 24-well plates containing 1 mL of DMEM. Explants were incubated at 32°C with gentle shaking (150 rpm) for 30 min. After incubation, the bath supernatant from the organ cultures was collected, and assayed to determine CGRP concentration with the CGRP EIA kit (Cayman Chemical) according to manufacturer's instructions.

Flow cytometry—Flank tissue samples of dermonecrotic lesions were dissected 24 h after infection, minced and incubated for 2 h (37°C, shaking) in 2 mL of HEPES-buffered saline (Sigma) containing collagenase A (1 mg/kg, Roche Applied Sciences) and dispase II (2.4 U/mL, Roche Applied Sciences). After incubation, cells were gently dissociated using a 16G needle attached to a 10 mL sterile syringe, filtered through a 70 µm mesh, and mixed with 20 mL of washing buffer constituted by HBSS (Thermo Fisher) and 0.5% BSA (Sigma). Cells were centrifuged for 5 min at 300g, supernatant was discarded, and the pellet was resuspended in 500 µL of washing buffer. The cell suspension was incubated on ice with mouse FcR Blocking Reagent (Miltenyi Biotec) for 10 min, and then incubated for 30 min on ice with the following antibodies: anti-CD45-APC/Cy7 (1:200, Biolegend), anti-Ly6G-A488 (1:200, Biolegend), anti-Ly6C-PerCP/Cy5.5 (1:200, Biolegend), anti-CD11b-BV605 (1:200, Biolegend), and Fixable Viability Dye eFluor-506 (1:1,200, Thermo Fisher). Cells were centrifuged for 5 min at 300g and the pellet resuspended in 500 µL of washing buffer/2% PFA. Flow cytometry was performed on a LSR II flow cytometer (BD Biosciences). Flow cytometry data were collected and exported using BD FACSDiva software (BD Biosciences). FACS data were analyzed and plotted using FlowJo software (FlowJo LLC).

QUANTIFICATION AND STATISTICAL ANALYSIS

Statistical analysis was performed, and results plotted using Graphpad Prism version 7.02 software. Data were represented as means±standard error of the mean (SEM) throughout the figures. The types of statistical analysis performed were based on standards in the fields of pain analysis and bacterial infection. Statistical comparisons of two groups for a single variable with normal distributions were analyzed by unpaired t-test. Statistical comparisons of three or more groups at a single time point were analyzed by One-way ANOVA with Tukey post-tests. Statistical comparisons of two or more groups with two independent variables were analyzed with Two-way ANOVA with Bonferroni post-tests. Statistical analysis of changes in two or more groups compared at multiple time points were analyzed by Two-way Repeated Measures ANOVA with Bonferroni post-tests performed at each time point. Below, we supply the exact details about the numbers of biological replicates, and types of statistical analysis used for the experiments found in each figure of the manuscript:

For Figure 1. (C) 4 mice per group were used for infection with M1 strain, and 9–11 mice per group were used for infection with M3 strain. (D) 8–9 mice per group were used for infection with M1 strain, and 7–10 mice per group were used for infection with M3 strain. (E) 8–9 mice per group were used for infection with M1 strain, and 7–9 mice per group were used for infection with M3 strain. (F) 3–4 plates containing 2,000 DRG neurons were used for each condition. One field per plate was imaged with a 20× objective and used for analysis. DRG neurons were obtained from a single mouse, and equally distributed across the groups tested. Statistical analysis: (C) One-way ANOVA, Tukey post-tests. (D–E) Two-way ANOVA, Bonferroni post-tests. (F) Two-way ANOVA, Bonferroni post-tests. (C, F) * $p < 0.05$ ** $p < 0.01$ *** $p < 0.001$ **** $p < 0.0001$. (D, E) veh vs 5×10^7 cfu: *** $p < 0.001$ **** $p < 0.0001$, veh vs 5×10^6 cfu: † $p < 0.05$ †† $p < 0.01$ ††† $p < 0.001$ †††† $p < 0.0001$, veh vs 5×10^5 cfu: §§ $p < 0.01$ §§§§ $p < 0.0001$.

For Figure 2. (A) 3–4 plates containing DRG neurons (2,000 cells per plate) from the same mouse were used for each condition. (C) 3 plates containing DRG neurons (2,000 cells per plate) from the same mouse were used for each condition. (D) 3 plates containing DRG neurons (2,000 cells per plate) from the same mouse were used for each condition. One field per plate was imaged with a 20× objective and used for analysis. (E) 5 wells containing DRG neurons (5,000 cells per well) were used for each condition. DRG neurons were obtained from 4 mice, pooled and equally distributed across the groups. Statistical analysis: (A) Two-way ANOVA, Bonferroni post-tests. (D, E) One-way ANOVA, Tukey post-tests. * $p < 0.05$ *** $p < 0.001$ **** $p < 0.0001$.

For Figure 3. (A, B) 8 mice per group were used for infection with M1 strains, and 12 mice per group were used for infection with M3 strains. (C) 10 mice per group were used. (D) 9–10 mice per group were used. (E) 4–5 mice per group were used. (F) 8 mice per group were used. Statistical analysis: (A, B, E, F) One-way ANOVA, Tukey post-tests, ** $p < 0.01$ *** $p < 0.001$ **** $p < 0.0001$; (C, D) Two-way ANOVA, Bonferroni post-tests, *sagA* vs wt * $p < 0.05$ *** $p < 0.001$ **** $p < 0.0001$, *slo sagA* vs wt †††† $p < 0.0001$.

For Figure 4. (A) 7–8 mice per group were used. (B) 5 mice per group were used. (C, D) 5 mice per group were used. (F) 14–16 mice per group were used. (H) 15 mice per group were used. Statistical analysis: (A–H) two-way ANOVA, Bonferroni post-tests. * $p < 0.05$ ** $p < 0.01$ *** $p < 0.001$ **** $p < 0.0001$. (B) *Tipv1-Cre/Dta* (ipsi) vs Control (ipsi). (D) RTX (ipsi) vs Veh (ipsi).

For Figure 5. (B, D) 4 mice per group were used. (E) 4–5 mice per group were used. (G, H) 3 mice per group were used. Statistical analysis: (B, D, E, H) Two-way ANOVA, Bonferroni post-tests. (G) One-way ANOVA, Tukey post-tests. * $p < 0.05$ ** $p < 0.01$ *** $p < 0.001$ **** $p < 0.0001$.

For Figure 6. (C) 10 mice per group were used. (D) 5–6 mice per group were used. (G, H) 6 mice per group were used. (I) 5 wells containing DRG neurons (5,000 cells per well) were used for each condition. DRG neurons were obtained from 2 mice, pooled, and equally distributed across the groups. (J) 3 mice per group were used to obtain skin punch biopsies, one biopsy per mouse. Statistical analysis: (C, D, G, H) Two-way ANOVA, Bonferroni post-

tests. (I, J) One-way ANOVA, Tukey post-tests. * $p < 0.05$ ** $p < 0.01$ *** $p < 0.001$ **** $p < 0.0001$.

For Figure 7. (A) 3–4 wells per group were used. DRG neurons (5,000 cells per well) were obtained from 2 mice, pooled, and equally distributed across the groups. Neutrophils (5×10^5 cells per well) were obtained from 4 mice, pooled, and equally distributed across the groups. (B) 4 wells per group were used. Neutrophils (5×10^5 cells per well) were obtained from 2 mice, pooled, and equally distributed across the groups. (C) 3 samples of human blood, obtained from 3 different donors, were used for all conditions. Each sample was tested in triplicate, and samples from different donors were not pooled. (D) 6–7 mice per group were used. (F, G) 10 mice per group were used. Statistical analysis: (A–C) One-way ANOVA, Tukey post-tests. (D–G) Two-way ANOVA, Bonferroni post-tests. (A–C, F–G) * $p < 0.05$ ** $p < 0.01$ *** $p < 0.001$ **** $p < 0.0001$. (D) BIBN4096 vs veh: * $p < 0.05$ ** $p < 0.01$ *** $p < 0.001$ **** $p < 0.0001$, BoNT/A vs veh: † $p < 0.05$ †† $p < 0.01$ ††† $p < 0.001$ †††† $p < 0.0001$.

For Figure S1. (A) 10 mice per group were used for infection with M1 strain, and 8–10 mice per group were used for infection with M3 strain. (B) 9–10 mice per group were used for infection with M1 strain, and 14–16 mice per group were used for infection with M3 strain. (C) 4 mice per group (time point) were used. (D) 8–12 mice per group were used. (E) 4 mice per group were used for infection with M1 strain, and 9–11 mice per group were used for infection with M3 strain (F) 3 mice per group were used, and 3 imaging fields of each mouse were used to quantify the average percentage. Statistical analysis: (A, D) Two-way ANOVA with Bonferroni post-tests (C, E, F) One-way ANOVA with Tukey post-tests. (A, C, D, E, F) * $p < 0.05$, ** $p < 0.01$, *** $p < 0.001$, **** $p < 0.0001$.

For Figure S2. (A) 5–6 mice per group were used. (B) 3 plates containing DRG neurons (2,000 cells per plate) from the same mouse were used for each condition. (C) 4 plates containing DRG neurons (2,000 cells per plate) from the same mouse were used for each condition. (D) 3 plates containing DRG neurons (2,000 cells per plate) from the same mouse were used for each condition. Statistical analysis: (A) Two-way ANOVA with Bonferroni post-tests. (B, C, D) One-way ANOVA with Tukey post-tests, * $p < 0.05$, ** $p < 0.01$, *** $p < 0.001$, **** $p < 0.0001$.

For Figure S3. (A) 3–6 wells containing DRG neurons (5,000 cells per well) were used for each condition. DRG neurons were obtained from 4 mice, pooled, and equally distributed across the groups. (B) 3 samples per group were used. (C, D) 8–12 mice per group were used. (E) 4–5 mice per group were used. Statistical analysis: (A–E) One-way ANOVA with Tukey post-tests. * $p < 0.05$, ** $p < 0.01$, *** $p < 0.001$, **** $p < 0.0001$.

For Figure S4. (A, C, D) 7 mice per group were used. (B) 4 mice per group were used. (E) 4–5 mice per group were used. (F) 3–5 mice per group were used, and 3 imaging fields of each mouse were used to quantify the average percentage. (G) 5 mice per group were used. (H) 3–4 mice per group were used and 3 imaging fields of each mouse were used to quantify the average percentage. Statistical analysis: (A, C, D) Two-way ANOVA with Bonferroni post-tests. (B) One-way ANOVA with Tukey post-tests. (E, F, G, H) Unpaired t-tests. ** $p < 0.01$, *** $p < 0.001$, **** $p < 0.0001$.

For Figure S5. (A) 14–16 mice per group were used. (C) 4 mice per group were used. (D) 3–4 mice per group were used to confirm neutrophil depletion. (E) 7–11 mice per group were used. (F) 7–11 mice per group were used for Abscess area measurements, and 10–11 mice per group were used for Mortality (Kaplan-Meier survival curves). Statistical analysis: (A, E, F) two-way ANOVA with Bonferroni post-tests, (C) one-way ANOVA with Tukey post-tests. (A, C) vehicle vs RTX = * $p < 0.05$, ** $p < 0.01$, *** $p < 0.001$, **** $p < 0.0001$. (E, F) RTX + IgG vs RTX + Gr1 = * $p < 0.05$, ** $p < 0.01$, *** $p < 0.001$, **** $p < 0.0001$.

For Figure S6. (A) 5–10 mice per group were used. (B) 6 mice per group were used. (C) 5 mice per group were used. (D) 6 mice per group were used. (E) 4–6 mice per group were used. (F) 5–10 mice per group were used. Statistical analysis: (A, C, E, F) two-way ANOVA with Bonferroni post-tests, (B, D) unpaired t-test. * $p < 0.05$, ** $p < 0.01$, *** $p < 0.001$, **** $p < 0.0001$.

For Figure S7. (A) 4 wells per group were used. Neutrophils (5×10^5 cells per well) were obtained from 4 mice, pooled, and equally distributed across the groups. (B) 4 wells per group were used. Neutrophils (5×10^5 cells per well) were obtained from 2 mice, pooled, and equally distributed across the groups. (C) 3–4 wells per group were used. Neutrophils (5×10^5 cells per well) were obtained from 4 mice, pooled, and equally distributed across the groups. (D) 6 mice per group were used. (E) 6–7 mice per group were used. (F) 4–5 mice per group were used. (G) 10 mice per group were used. Statistical analysis: (A, C, D, F) One-way ANOVA with Tukey post-tests, (B) Unpaired t-test, (E, G) Two-way ANOVA with Bonferroni post-tests. * $p < 0.05$, ** $p < 0.01$, **** $p < 0.0001$. (E) BIBN4096 vs vehicle = ** $p < 0.01$, **** $p < 0.0001$; BoNT/A vs vehicle († $p < 0.05$, †† $p < 0.01$, ††† $p < 0.0001$).

Supplementary Material

Refer to Web version on PubMed Central for supplementary material.

Acknowledgments

We thank Ernest Aw, Maria Izabella Alves, Yibing Wei, Pankaj Baral, Chad Araneo, Kaitlin Goldstein, Tammy Hshieh and Erica Alexandre for support. This work was supported by NIH grants DP2AT009499 and RO1AI130019 to IMC, RO1AI070926 and RO1AI029952 to MRW, RO1AI010085 and R21AI116808 to JBD, CAPES fellowship to FAPR, CNPq Researcher fellowship 307186/2017-2 to WAVJ.

References

- Abraira VE, Ginty DD. The Sensory Neurons of Touch. *Neuron*. 2013; 79:618–639. [PubMed: 23972592]
- Ashbaugh CD, Warren HB, Carey VJ, Wessels MR. Molecular analysis of the role of the group A streptococcal cysteine protease, hyaluronic acid capsule, and M protein in a murine model of human invasive soft-tissue infection. *J. Clin. Invest.* 1998; 102:550–560. [PubMed: 9691092]
- Bastiat-Sempe B, Love JF, Lomayeva N, Wessels MR. Streptolysin O and NAD-glycohydrolase prevent phagolysosome acidification and promote group A Streptococcus survival in macrophages. *MBio* 5. 2014:e01690–14.
- Basbaum AI, Bautista DM, Scherrer G, Julius D. Cellular and molecular mechanisms of pain. *Cell*. 2009; 139:267–284. [PubMed: 19837031]

- Bellono NW, Bayrer JR, Leitch DB, Castro J, Zhang C, O'Donnell TA, Brierley SM, Ingraham HA, Julius D. Enterochromaffin Cells Are Gut Chemosensors that Couple to Sensory Neural Pathways. *Cell*. 2017; 170:185–198.e16. [PubMed: 28648659]
- Bentley CC, Hakansson A, Christianson J, Wessels MR. Extracellular group A Streptococcus induces keratinocyte apoptosis by dysregulating calcium signalling. *Cell. Microbiol.* 2005; 7:945–955. [PubMed: 15953027]
- Betschel SD, Borgia SM, Barg NL, Low DE, De Azavedo JCS. Reduced Virulence of Group A Streptococcal Tn916 Mutants That Do Not Produce Streptolysin S. *Infect. Immun.* 1998; 66:1671–1679. [PubMed: 9529097]
- Binshtok AM, Wang H, Zimmermann K, Amaya F, Vardeh D, Shi L, Brenner GJ, Ji R-R, Bean BP, Woolf CJ, et al. Nociceptors are interleukin-1beta sensors. *J. Neurosci.* 2008; 28:14062–14073. [PubMed: 19109489]
- Binz T, Blasi J, Yamasaki S, Baumeister A, Link E, Südhof TC, Jahn R, Niemann H. Proteolysis of SNAP-25 by types E and A botulinum neurotoxins. *J. Biol. Chem.* 1994; 269:1617–1620. [PubMed: 8294407]
- Borschitz T, Schlicht S, Siegel E, Hanke E, von Stebut E, Goldberg E. Improvement of a Clinical Score for Necrotizing Fasciitis: “Pain Out of Proportion” and High CRP Levels Aid the Diagnosis. *PLoS One.* 2015; 10:e0132775. [PubMed: 26196941]
- Bricker AL, Cywes C, Ashbaugh CD, Wessels MR. NAD⁺-glycohydrolase acts as an intracellular toxin to enhance the extracellular survival of group A streptococci. *Mol. Microbiol.* 2002; 44:257–269. [PubMed: 11967084]
- Buchanan CS, Haserick JR. Necrotizing fasciitis due to group A beta-hemolytic streptococci. *Arch. Dermatol.* 1970; 101:664–668. [PubMed: 5424482]
- Caceres AI, Brackmann M, Elia MD, Bessac BF, del Camino D, D'Amours M, Witek JS, Fanger CM, Chong Ja, Hayward NJ, et al. A sensory neuronal ion channel essential for airway inflammation and hyperreactivity in asthma. *Proc. Natl. Acad. Sci. U. S. A.* 2009; 106:9099–9104. [PubMed: 19458046]
- Chavan SS, Pavlov VA, Tracey KJ. Mechanisms and Therapeutic Relevance of Neuro-immune Communication. *Immunity.* 2017; 46:927–942. [PubMed: 28636960]
- Chiu IM, Heesters BA, Ghasemlou N, Von Hehn CA, Zhao F, Tran J, Wainger B, Strominger A, Muralidharan S, Horswill AR, et al. Bacteria activate sensory neurons that modulate pain and inflammation. *Nature.* 2013; 501:52–57. [PubMed: 23965627]
- Chiu IM, Barrett LB, Williams EK, Strohlic DE, Lee S, Weyer AD, Lou S, Bryman GS, Roberson DP, Ghasemlou N, et al. Transcriptional profiling at whole population and single cell levels reveals somatosensory neuron molecular diversity. *Elife.* 2014; 3
- Cole JN, Barnett TC, Nizet V, Walker MJ. Molecular insight into invasive group A streptococcal disease. *Nat. Rev. Microbiol.* 2011; 9:724–736. [PubMed: 21921933]
- Dale JB, Chiang EY, Hasty DL, Courtney HS. Antibodies against a synthetic peptide of SagA neutralize the cytolytic activity of streptolysin S from group A streptococci. *Infect. Immun.* 2002; 70:2166–2170. [PubMed: 11895983]
- Datta V, Myskowski SM, Kwinn LA, Chiem DN, Varki N, Kansal RG, Kotb M, Nizet V. Mutational analysis of the group A streptococcal operon encoding streptolysin S and its virulence role in invasive infection. *Mol. Microbiol.* 2005; 56:681–695. [PubMed: 15819624]
- Flaherty RA, Puricelli JM, Higashi DL, Park CJ, Lee SW. Streptolysin S Promotes Programmed Cell Death and Enhances Inflammatory Signaling in Epithelial Keratinocytes during Group A Streptococcus Infection. *Infect. Immun.* 2015; 83:4118–4133. [PubMed: 26238711]
- Gabanyi I, Muller PA, Feighery L, Oliveira TY, Costa-Pinto FA, Mucida D. Neuro-immune Interactions Drive Tissue Programming in Intestinal Macrophages. *Cell.* 2016; 164:378–391. [PubMed: 26777404]
- Gilbert E, W N. Efficacy of botulinum neurotoxin type A for treating recalcitrant plaque psoriasis. *J. Drugs Dermatol.* 2014; 13:1407–1408. [PubMed: 25607710]
- Grando SA, Zachary CB. THE NON-NEURONAL AND NON-MUSCULAR EFFECTS OF BOTULINUM TOXIN: A Graceful Opportunity for a Deadly Molecule to Treat a Human Disease in the Skin and Beyond. *Br. J. Dermatol.* 2017

- Granstein RD, Wagner JA, Stohl LL, Ding W. Calcitonin gene-related peptide: key regulator of cutaneous immunity. *Acta Physiol. (Oxf)*. 2015; 213:586–594. [PubMed: 25534428]
- Gryllos I, Tran-Winkler HJ, Cheng M-F, Chung H, Bolcome R, Lu W, Lehrer RI, Wessels MR, Wessels MR. Induction of group A Streptococcus virulence by a human antimicrobial peptide. *Proc. Natl. Acad. Sci. U. S. A.* 2008; 105:16755–16760. [PubMed: 18936485]
- Higashi DL, Biais N, Donahue DL, Mayfield JA, Tessier CR, Rodriguez K, Ashfeld BL, Luchetti J, Ploplis VA, Castellino FJ, et al. Activation of band 3 mediates group A Streptococcus streptolysin S-based beta-haemolysis. *Nat. Microbiol.* 2016; 1:15004. [PubMed: 27571972]
- Hou Q, Barr T, Gee L, Vickers J, Wymer J, Borsani E, Rodella L, Getsios S, Burdo T, Eisenberg E, et al. Keratinocyte expression of calcitonin gene-related peptide β : Implications for neuropathic and inflammatory pain mechanisms. *Pain*. 2011; 152:2036–2051. [PubMed: 21641113]
- Hunskar S, Fasmer OB, Hole K. Formalin test in mice, a useful technique for evaluating mild analgesics. *J. Neurosci. Methods*. 1985; 14:69–76. [PubMed: 4033190]
- Ji Y, McLandsborough L, Kondagunta A, Cleary PP. C5a peptidase alters clearance and trafficking of group A streptococci by infected mice. *Infect. Immun.* 1996; 64:503–510. [PubMed: 8550199]
- Kashem SW, Riedl MS, Yao C, Honda CN, Vulchanova L, Kaplan DH. Nociceptive Sensory Fibers Drive Interleukin-23 Production from CD301b+ Dermal Dendritic Cells and Drive Protective Cutaneous Immunity. *Immunity*. 2015; 43:515–526. [PubMed: 26377898]
- Krämer HH, Angerer C, Erbguth F, Schmelz M, Birklein F. Botulinum Toxin A reduces neurogenic flare but has almost no effect on pain and hyperalgesia in human skin. *J. Neurol.* 2003; 250:188–193. [PubMed: 12574949]
- Kurupati P, Turner CE, Tziona I, Lawrenson RA, Alam FM, Nohadani M, Stamp GW, Zinkernagel AS, Nizet V, Edwards RJ, et al. Chemokine-cleaving Streptococcus pyogenes protease SpyCEP is necessary and sufficient for bacterial dissemination within soft tissues and the respiratory tract. *Mol. Microbiol.* 2010; 76:1387–1397. [PubMed: 20158613]
- Lee W-H, Shin TJ, Kim HJ, Lee J-K, Suh H-W, Lee SC, Seo K. Intrathecal Administration of Botulinum Neurotoxin Type A Attenuates Formalin-Induced Nociceptive Responses in Mice. *Anesth. Analg.* 2011; 112:228–235. [PubMed: 21081780]
- Leitch HA, Palepu A, Fernandes CM. Necrotizing fasciitis secondary to group A streptococcus. Morbidity and mortality still high. *Can. Fam. Physician*. 2000; 46:1460–1466. [PubMed: 10925760]
- Lin A, Loughman JA, Zinselmeyer BH, Miller MJ, Caparon MG. Streptolysin S inhibits neutrophil recruitment during the early stages of Streptococcus pyogenes infection. *Infect. Immun.* 2009; 77:5190–5201. [PubMed: 19687200]
- Liu B, Escalera J, Balakrishna S, Fan L, Caceres AI, Robinson E, Sui A, McKay MC, McAlexander MA, Herrick CA, et al. TRPA1 controls inflammation and pruritogen responses in allergic contact dermatitis. *FASEB J.* 2013; 27:3549–3563. [PubMed: 23722916]
- Love JF, Tran-Winkler HJ, Wessels MR. Vitamin D and the human antimicrobial peptide LL-37 enhance group a streptococcus resistance to killing by human cells. *MBio.* 2012; 3:e00394–12. [PubMed: 23093388]
- Martinon F, Burns K, Tschopp J. The inflammasome: a molecular platform triggering activation of inflammatory caspases and processing of proIL-beta. *Mol. Cell.* 2002; 10:417–426. [PubMed: 12191486]
- Meng J, Wang J, Lawrence G, Dolly JO. Synaptobrevin I mediates exocytosis of CGRP from sensory neurons and inhibition by botulinum toxins reflects their anti-nociceptive potential. *J. Cell Sci.* 2007; 120:2864–2874. [PubMed: 17666428]
- Mishra SK, Tisel SM, Orestes P, Bhangoo SK, Hoon MA. TRPV1-lineage neurons are required for thermal sensation. *EMBO J.* 2011; 30:582–593. [PubMed: 21139565]
- Molloy EM, Cotter PD, Hill C, Mitchell DA, Ross RP. Streptolysin S-like virulence factors: the continuing saga. *Nat. Rev. Microbiol.* 2011; 9:670–681. [PubMed: 21822292]
- Muller PA, Koscsó B, Rajani GM, Stevanovic K, Berres ML, Hashimoto D, Mortha A, Leboeuf M, Li XM, Mucida D, et al. Crosstalk between muscularis macrophages and enteric neurons regulates gastrointestinal motility. *Cell.* 2014; 158:300–313. [PubMed: 25036630]

- Nizet V. Streptococcal beta-hemolysins: genetics and role in disease pathogenesis. *Trends Microbiol.* 2002; 10:575–580. [PubMed: 12564994]
- Nizet V, Beall B, Bast DJ, Datta V, Kilburn L, Low DE, De Azavedo JC. Genetic locus for streptolysin S production by group A streptococcus. *Infect. Immun.* 2000; 68:4245–4254. [PubMed: 10858242]
- Oetjen LK, Mack MR, Feng J, Whelan TM, Niu H, Guo CJ, Chen S, Trier AM, Xu AZ, Tripathi SV, et al. Sensory Neurons Co-opt Classical Immune Signaling Pathways to Mediate Chronic Itch. *Cell.* 2017; 171:217–228.e13. [PubMed: 28890086]
- Olsen RJ, Musser JM. Molecular Pathogenesis of Necrotizing Fasciitis. *Annu. Rev. Pathol. Mech. Dis.* 2010; 5:1–31.
- O'Seaghda M, Wessels MR. Streptolysin O and its co-toxin NAD-glycohydrolase protect group A Streptococcus from Xenophagic killing. *PLoS Pathog.* 2013; 9:e1003394. [PubMed: 23762025]
- Okumura CYM, Nizet V. Subterfuge and Sabotage: Evasion of Host Innate Defenses by Invasive Gram-Positive Bacterial Pathogens. *Annu. Rev. Microbiol.* 2014; 68:439–458. [PubMed: 25002085]
- Perez-Casal J, Price JA, Maguin E, Scott JR. An M protein with a single C repeat prevents phagocytosis of Streptococcus pyogenes: use of a temperature-sensitive shuttle vector to deliver homologous sequences to the chromosome of S. pyogenes. *Mol. Microbiol.* 1993; 8:809–819. [PubMed: 8355608]
- Petersen KA, Lassen LH, Birk S, Lesko L, Olesen J. BIBN4096BS Antagonizes Human α -calcitonin Gene Related Peptide–induced Headache and Extracerebral Artery Dilatation*. *Clin. Pharmacol. Ther.* 2005; 77:202–213. [PubMed: 15735614]
- Pinho-Ribeiro FA, Verri WA, Chiu IM. Nociceptor Sensory Neuron–Immune Interactions in Pain and Inflammation. *Trends Immunol.* 2017; 38
- Ralph AP, Carapetis JR. Group A streptococcal diseases and their global burden. *Curr. Top. Microbiol. Immunol.* 2013; 368:1–27. [PubMed: 23242849]
- Riol-Blanco L, Ordovas-Montanes J, Perro M, Naval E, Thiriote A, Alvarez D, Paust S, Wood JN, von Andrian UH. Nociceptive sensory neurons drive interleukin-23-mediated psoriasiform skin inflammation. *Nature.* 2014; 510:157–161. [PubMed: 24759321]
- Rainsford KD. Fifty years of ibuprofen: advancing pain and fever management. *Int. J. Clin. Pract.* 2013; 67:1–2.
- Romero M, Keyel M, Shi G, Bhattacharjee P, Roth R, Heuser JE, Keyel PA. Intrinsic repair protects cells from pore-forming toxins by microvesicle shedding. *Cell Death Differ.* 2017; 24:798–808. [PubMed: 28186501]
- Schrager HM, Rheinwald JG, Wessels MR. Hyaluronic acid capsule and the role of streptococcal entry into keratinocytes in invasive skin infection. *J. Clin. Invest.* 1996; 98:1954–1958. [PubMed: 8903312]
- Shinkai Y, Rathbun G, Lam KP, Oltz EM, Stewart V, Mendelsohn M, Charron J, Datta M, Young F, Stall AM. RAG-2-deficient mice lack mature lymphocytes owing to inability to initiate V(D)J rearrangement. *Cell.* 1992; 68:855–867. [PubMed: 1547487]
- Sierig G, Cywes C, Wessels MR, Ashbaugh CD. Cytotoxic effects of streptolysin o and streptolysin s enhance the virulence of poorly encapsulated group a streptococci. *Infect. Immun.* 2003; 71:446–455. [PubMed: 12496195]
- Stevens DL, Bryant AE. Necrotizing Soft-Tissue Infections. *N. Engl. J. Med.* 2017; 377:2253–2265. [PubMed: 29211672]
- Takahashi K, Nakanishi S, Imamura S. Direct effects of cutaneous neuropeptides on adenylyl cyclase activity and proliferation in a keratinocyte cell line: Stimulation of cyclic AMP formation by CGRP and VIP/PHM, and inhibition by NPY through G protein-coupled receptors. *J. Invest. Dermatol.* 1993; 101:646–651. [PubMed: 8228323]
- Talbot S, Abdulnour R-EE, Burkett PR, Lee S, Cronin SJF, Pascal MA, Laedermann C, Foster SL, Tran JV, Lai N, et al. Silencing Nociceptor Neurons Reduces Allergic Airway Inflammation. *Neuron.* 2015; 87:341–354. [PubMed: 26119026]
- Thulin P, Johansson L, Low DE, Gan BS, Kotb M, McGeer A, Norrby-Teglund A. Viable group A streptococci in macrophages during acute soft tissue infection. *PLoS Med.* 2006; 3:371–379.

- Tso AR, Goadsby PJ. Anti-CGRP Monoclonal Antibodies: the Next Era of Migraine Prevention? *Curr. Treat. Options Neurol.* 2017; 19:27. [PubMed: 28653227]
- Tweten RK, Hotze EM, Wade KR. The Unique Molecular Choreography of Giant Pore Formation by the Cholesterol-Dependent Cytolysins of Gram-Positive Bacteria. *Annu. Rev. Microbiol.* 2015; 69:323–340. [PubMed: 26488276]
- Veiga-Fernandes H, Mucida D. Neuro-Immune Interactions at Barrier Surfaces. *Cell.* 2016; 165:801–811. [PubMed: 27153494]
- Wilson HD, Haltalin KC. Acute necrotizing fasciitis in childhood. Report of 11 cases. *Am. J. Dis. Child.* 1973; 125:591–595. [PubMed: 4633570]
- Wilson SR, Thé L, Batia LM, Beattie K, Katibah GE, McClain SP, Pellegrino M, Estandian DM, Bautista DM. The Epithelial Cell-Derived Atopic Dermatitis Cytokine TSLP Activates Neurons to Induce Itch. *Cell.* 2013a; 155:285–295. [PubMed: 24094650]
- Wilson SR, Nelson AM, Batia L, Morita T, Estandian D, Owens DM, Lumpkin EA, Bautista DM. The Ion Channel TRPA1 Is Required for Chronic Itch. *J. Neurosci.* 2013b; 33:9283–9294. [PubMed: 23719797]
- Yamamoto M, Sato S, Hemmi H, Hoshino K, Kaisho T, Sanjo H, Takeuchi O, Sugiyama M, Okabe M, Takeda K, et al. Role of Adaptor TRIF in the MyD88-Independent Toll-Like Receptor Signaling Pathway. *Science.* 2003; 301:640–643. [PubMed: 12855817]

HIGHLIGHTS

- *S. pyogenes* produces pain during bacterial invasion through Streptolysin S (SLS).
- SLS induces TRPV1 neurons to release the neuropeptide CGRP in infected tissues.
- Neurons suppress neutrophil recruitment and bactericidal activity.
- BoNT/A and CGRP antagonist block neural suppression of immunity to treat infection.

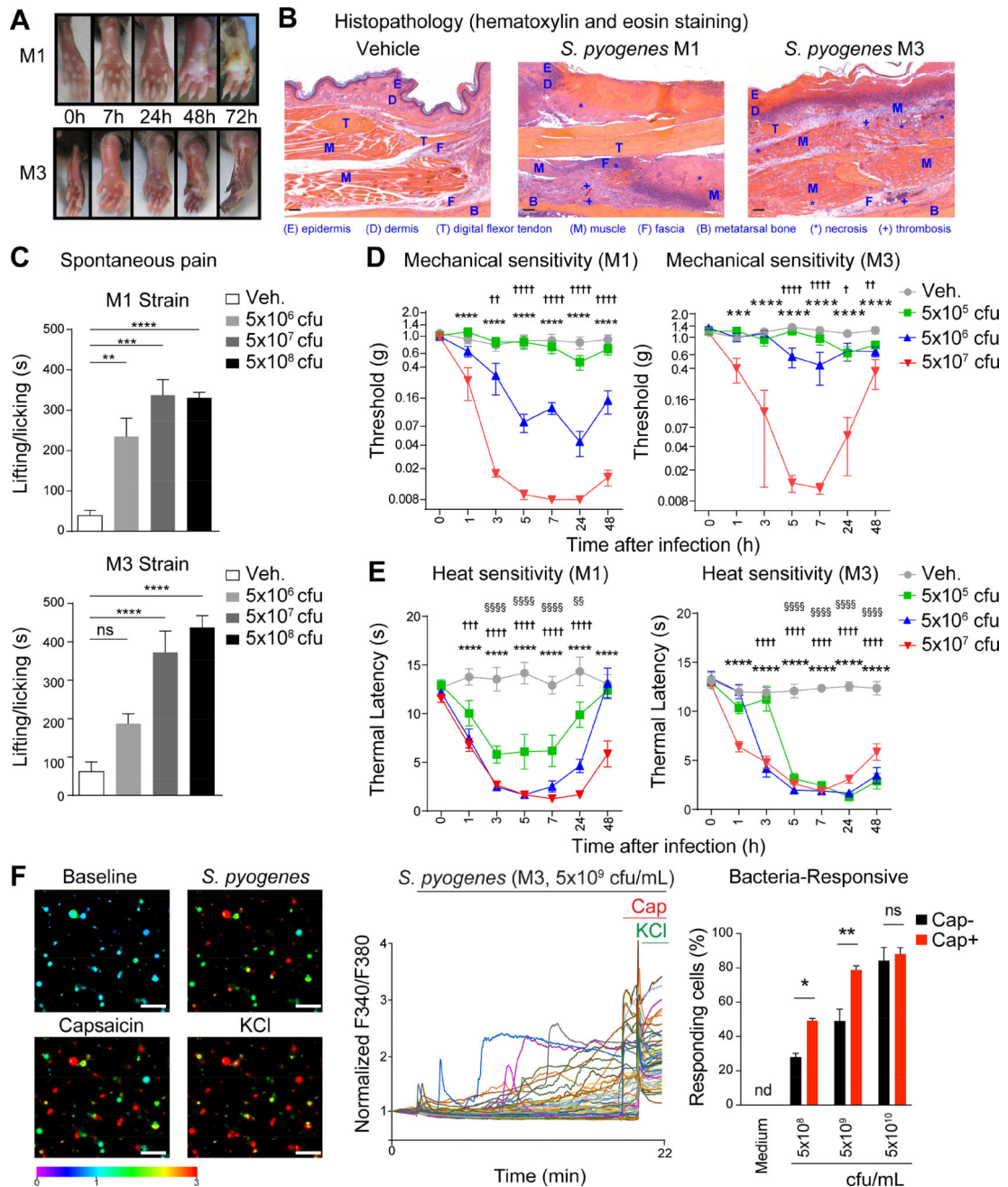


Figure 1. *S. pyogenes* induces pain associated behaviors and directly activates sensory neurons (A) Representative images of mouse hind paws at different time points after subcutaneous injection of *S. pyogenes* M1 or M3 strains (5×10^7 cfu). (B) Histopathology of skin and soft tissue biopsies 72 h after injection of vehicle, M1 or M3 (5×10^7 cfu). Scale bars, 100 μ m. (C) Spontaneous pain reflexes (lifting/licking of hind paw) over 1 h after injection of different inoculums of M1 (n=4/group) or M3 (n=9–11/group). (D) Mechanical sensitivity after injection of vehicle, *S. pyogenes* M1 (n=8–9/group) or M3 (n=7–10/group). (E) Heat sensitivity after injection of vehicle, *S. pyogenes* M1 (n=8–9/group) or M3 (n=7–9/group). (F) Representative Fura-2 ratiometric fields (Left) and calcium traces (Center) of DRG

neurons at baseline and after stimulation *in vitro* with live *S. pyogenes* M3 (5×10^9 cfu/mL), capsaicin (1 μ m), and KCl (40 mM). Scale bars, 50 μ m. Proportions (Right) of capsaicin non-responsive (Cap-) and capsaicin responsive (Cap+) neurons that responded to M3 (n=3–4 fields/condition). Statistical analysis: (C) One-way ANOVA, Tukey post-tests. (D–E) Two-way ANOVA, Bonferroni post-tests. (F) Two-way ANOVA, Bonferroni post-tests. (C,F) *p<0.05 **p<0.01 ***p<0.001 ****p<0.0001. (D,E) veh vs 5×10^7 cfu: ***p<0.001 ****p<0.0001, veh vs 5×10^6 cfu: †p<0.05 ††p<0.01 †††p<0.001 ††††p<0.0001, veh vs 5×10^5 cfu: §§p<0.01 §§§§p<0.0001. ns=not significant. Mean \pm SEM. See Figure S1 for related data.

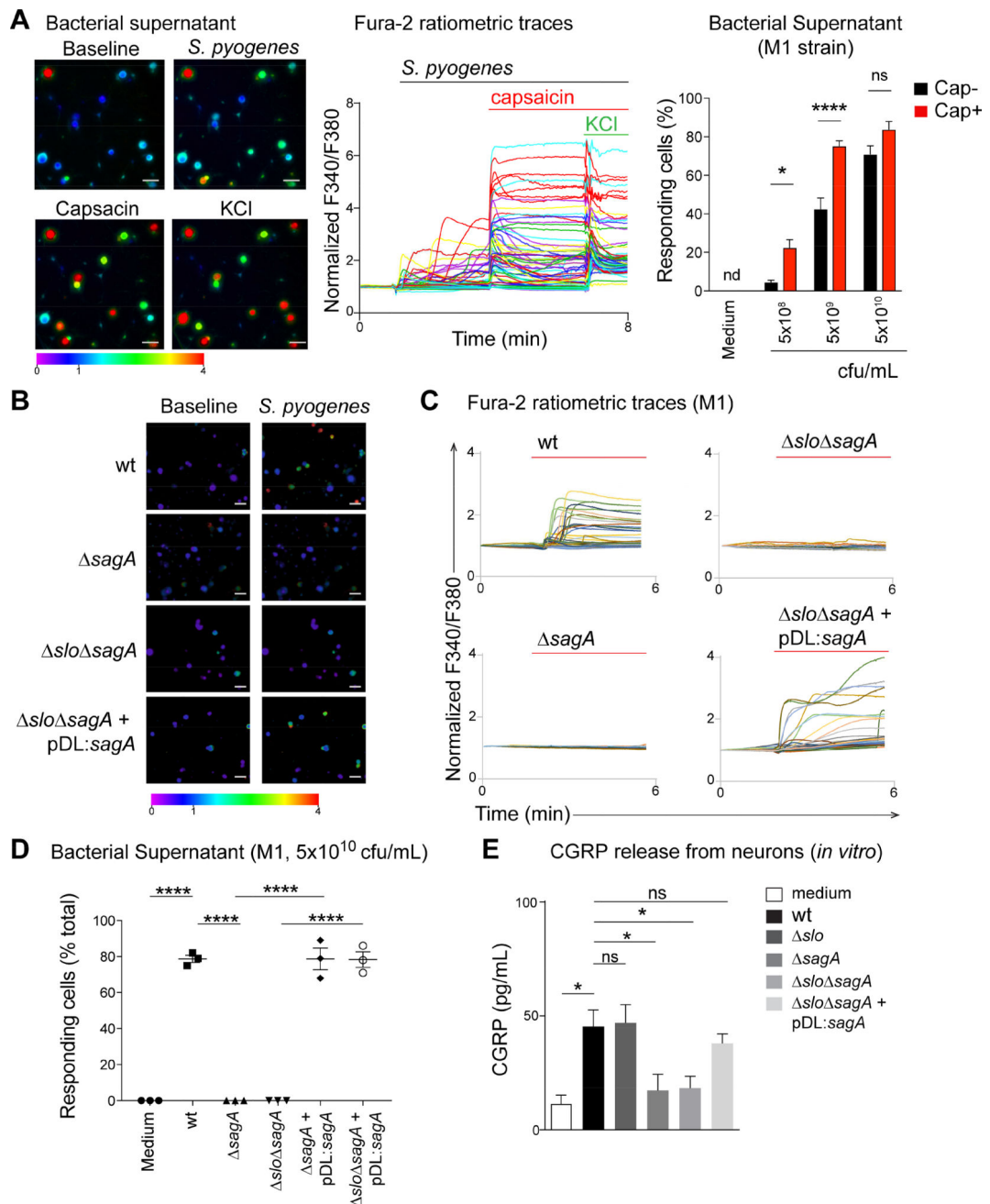


Figure 2. *S. pyogenes* induces neuronal activation and CGRP release through SLS
(A) Representative Fura-2 ratiometric fields (left) and calcium traces (center) of DRG neurons responding to filtered supernatant from *S. pyogenes* M1 (5x10⁹ cfu/mL), capsaicin (1 μm), and KCl (40 mM). Proportions (Right) of capsaicin non-responsive (Cap-) and capsaicin responsive (Cap+) neurons that responded to M1 supernatant (n=3–4 fields/condition). **(B–D)** Representative Fura-2 ratiometric fields **(B)** and calcium traces **(C)** of DRG neurons stimulated with filtered supernatant from *S. pyogenes* M1 (wt) or isogenic mutants lacking SLS (*sagA*), both SLO and SLS (*slo sagA*), or double mutant bacteria in which *sagA* expression was restored (*slo sagA*+pDL:*sagA*). **(D)** Proportions of

responding DRG neurons to bacterial supernatant from *S. pyogenes* M1 (wt) or isogenic mutant strains (n=3 fields/condition). (E) DRG neurons stimulated for 30 min with supernatant from *S. pyogenes* M1 (wt), isogenic mutants, or medium, analyzed for *in vitro* release of CGRP (n=5 samples/group). Statistical analysis: (A) Two-way ANOVA, Bonferroni post-tests. (D,E) One-way ANOVA, Tukey post-tests. *p<0.05 ***p<0.001 ****p<0.0001. ns=not significant. Scale bars, 50 μ m. Mean \pm SEM. See Figure S2 for related data.

Author Manuscript

Author Manuscript

Author Manuscript

Author Manuscript

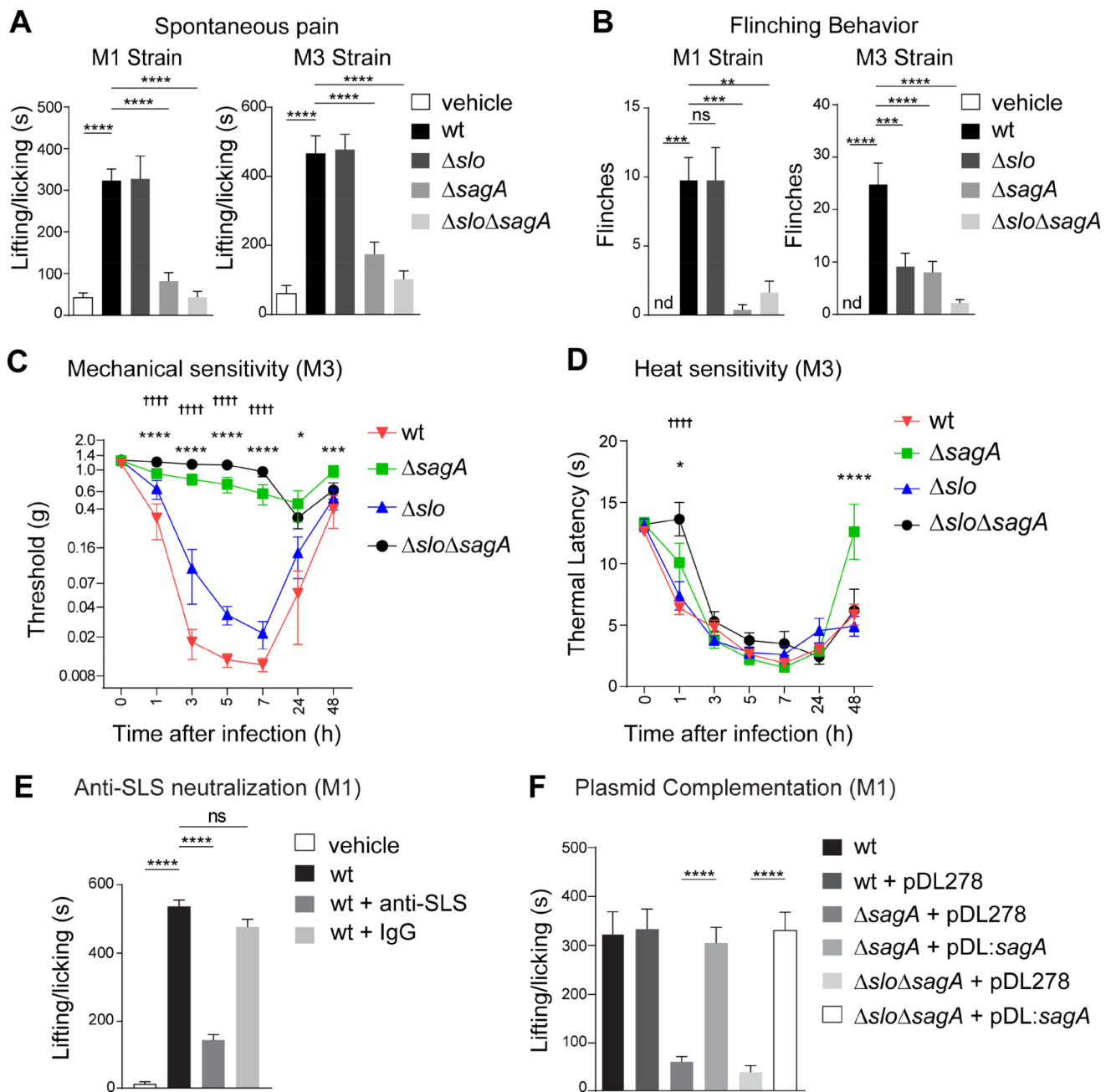


Figure 3. SLS is necessary for pain during *S. pyogenes* infection

(A,B) Spontaneous lifting/licking pain over 1 h after injection of vehicle, *S. pyogenes* M1 or M3 (5×10^8 cfu) wt, *sagA*, *slo*, or *slo sagA* strains (M1, n=8/group; M3, n=12/group). (C,D) Mechanical (n=10/group) and heat (n=9–10/group) sensitivity after injection of *S. pyogenes* M3 wt or isogenic mutants (5×10^7 cfu). (E) Spontaneous pain over 1 h in mice injected with *S. pyogenes* M1 (5×10^8 cfu) and treated with anti-SLS or control IgG (n=4–5/group). (F) Spontaneous pain over 1 h after injection of *S. pyogenes* M1 (5×10^8 cfu) wt or isogenic mutants complemented with plasmid encoding *sagA* (pDL:sagA) or empty plasmid (pDL278) (n=8/group). Statistical analysis: (A,B,E,F) One-way ANOVA, Tukey post-tests, **p<0.01 ***p<0.001 ****p<0.0001; (C,D) Two-way ANOVA, Bonferroni post-tests,

sagA vs wt * $p < 0.05$ *** $p < 0.001$ **** $p < 0.0001$, *slo sagA* vs wt †††† $p < 0.0001$. ns=not significant. nd=not detected. Mean±SEM. See Figure S3 for related data.

Author Manuscript

Author Manuscript

Author Manuscript

Author Manuscript

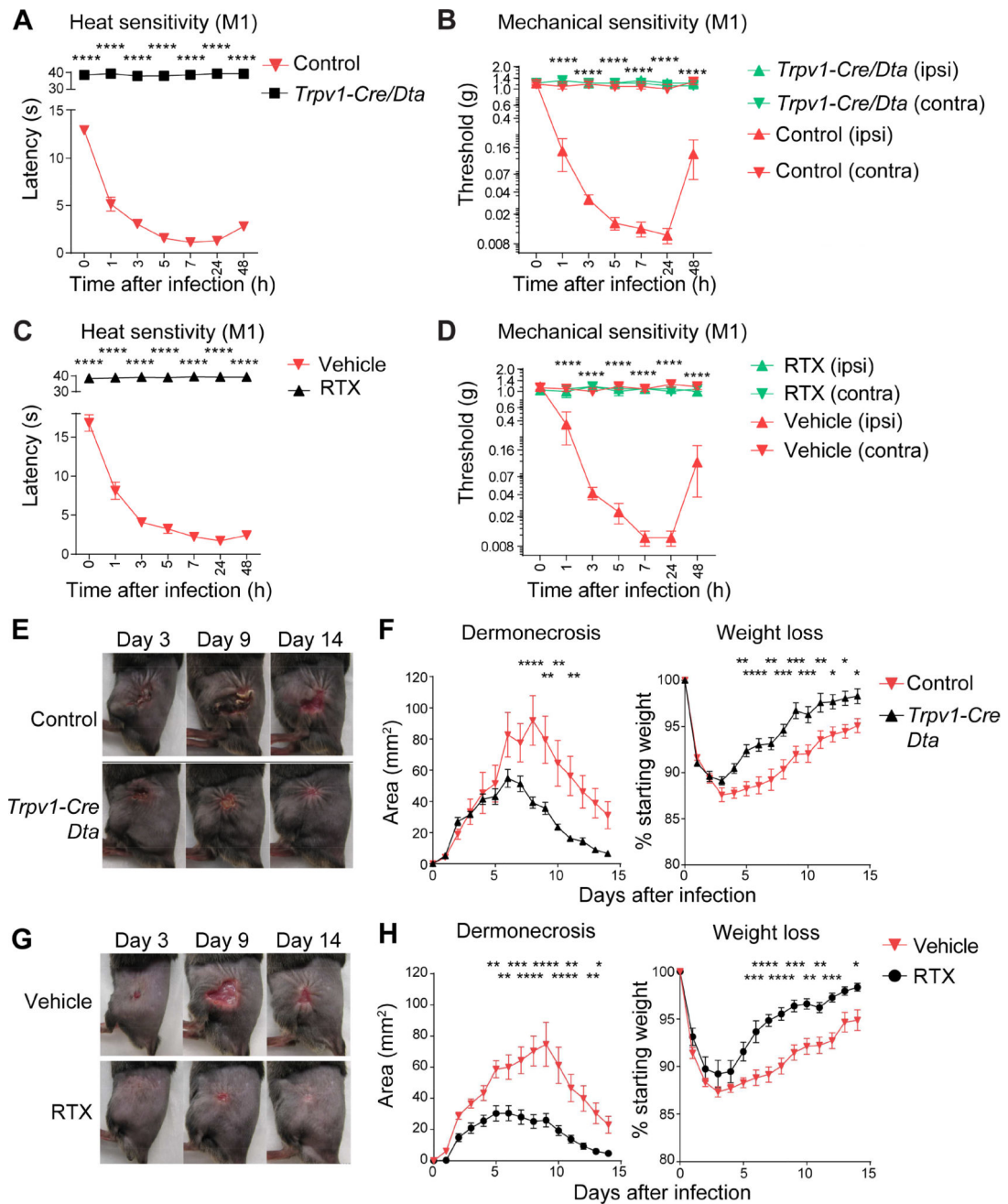


Figure 4. TRPV1 neurons that mediate pain inhibit host defenses against *S. pyogenes* infection (A) Heat sensitivity measured in *Trpv1-Cre/Dta* mice and control littermates after *S. pyogenes* M1 injection (5×10^7 cfu, n=7-8/group). (B) Mechanical sensitivity of ipsilateral (ipsi) and contralateral (contra) hind paws after *S. pyogenes* M1 injection (5×10^7 cfu) in *Trpv1-Cre/Dta* and control littermates (n=5/group). (C) Heat sensitivity in RTX and vehicle-treated mice after *S. pyogenes* M1 injection (5×10^7 cfu, n=5/group). (D) Mechanical sensitivity of ipsilateral and contralateral hind paws of RTX and vehicle-treated mice after *S. pyogenes* M1 injection (5×10^7 cfu, n=5/group). (E-H) *S. pyogenes* M1 (5×10^6 cfu) was injected subcutaneously into the flank of mice: (E) Representative pictures of flank lesions,

and **(F)** Quantification of dermonecrosis and weight loss at different time points after *S. pyogenes* M1 injection in *Trpv1-Cre/Dta* or control littermates (n=14–16/group). **(G)** Representative pictures of flank lesions, and **(H)** Quantification of dermonecrosis and weight loss after *S. pyogenes* M1 injection in RTX or vehicle-treated mice (n=15/group). Statistical analysis: **(A–H)** two-way ANOVA, Bonferroni post-tests. *p<0.05 **p<0.01 ***p<0.001 ****p<0.0001. **(B)** *Trpv1-Cre/Dta* (ipsi) vs Control (ipsi). **(D)** RTX (ipsi) vs Veh (ipsi). Mean±SEM. See Figure S4 for related data.

Author Manuscript

Author Manuscript

Author Manuscript

Author Manuscript

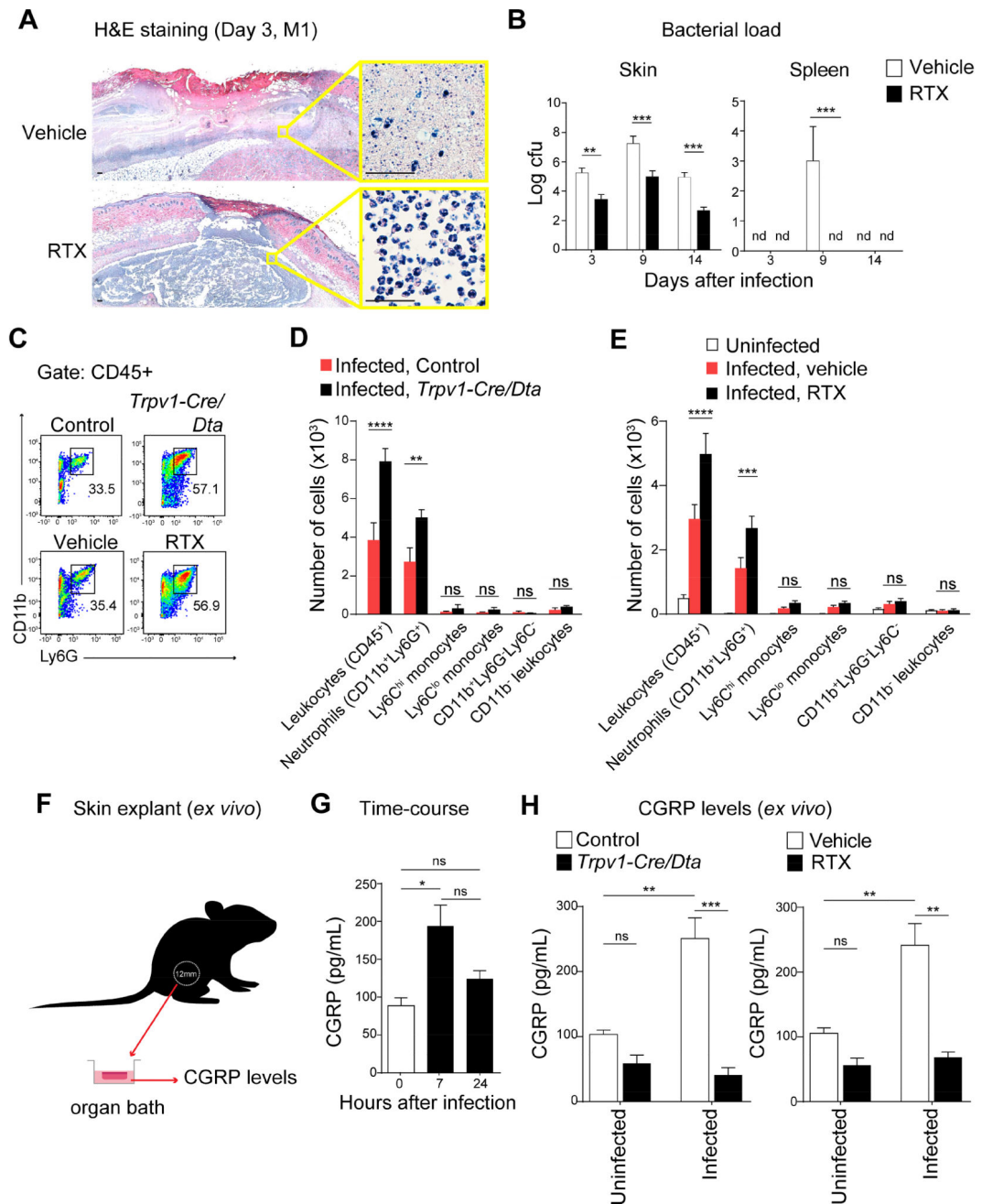


Figure 5. Nociceptors suppress recruitment of neutrophils that mediate host protection against *S. pyogenes* infection

(A) Histopathology of flank biopsies from vehicle or RTX-treated mice 3 days after injection of *S. pyogenes* M1 (5×10^6 cfu). Scale bars, 50 μ m. (B) Bacterial load recovery (\log_{10} cfu) from flank lesions and spleens in RTX or vehicle-treated mice after *S. pyogenes* M1 injection (5×10^6 cfu, n=4/group). (C–E) Flow cytometry of leukocyte recruitment in necrotizing lesions 1 day after *S. pyogenes* M1 injection (5×10^6 cfu): (C) Representative FACS plots showing neutrophils (CD11b⁺Ly6G⁺ gates) in lesion samples. (D–E) Quantification of immune cell populations by flow cytometry in flank biopsies from infected

Trpv1-Cre/Dta mice or control littermates (n=4/group), or from uninfected mice, infected vehicle-treated mice, or infected RTX-treated mice (n=4–5/group). **(F–H)** Measurement of CGRP release *ex vivo* from flank skin punch biopsies. **(G)** CGRP release from uninfected skin (0 h), 7 h, or 24 h after *S. pyogenes* M1 injection (5×10^6 cfu) (n=3/group). **(H)** CGRP release from uninfected skin or 7 h after *S. pyogenes* M1 (5×10^6 cfu) injection of *Trpv1-Cre/Dta* mice or control littermates, or Vehicle or RTX-treated mice (n=3/group). Statistical analysis: **(B,D,E,H)** Two-way ANOVA, Bonferroni post-tests. **(G)** One-way ANOVA, Tukey post-tests. *p<0.05 **p<0.01 ***p<0.001 ****p<0.0001. ns=not significant. nd=none detected. Mean±SEM. See Figure S5 for related data.

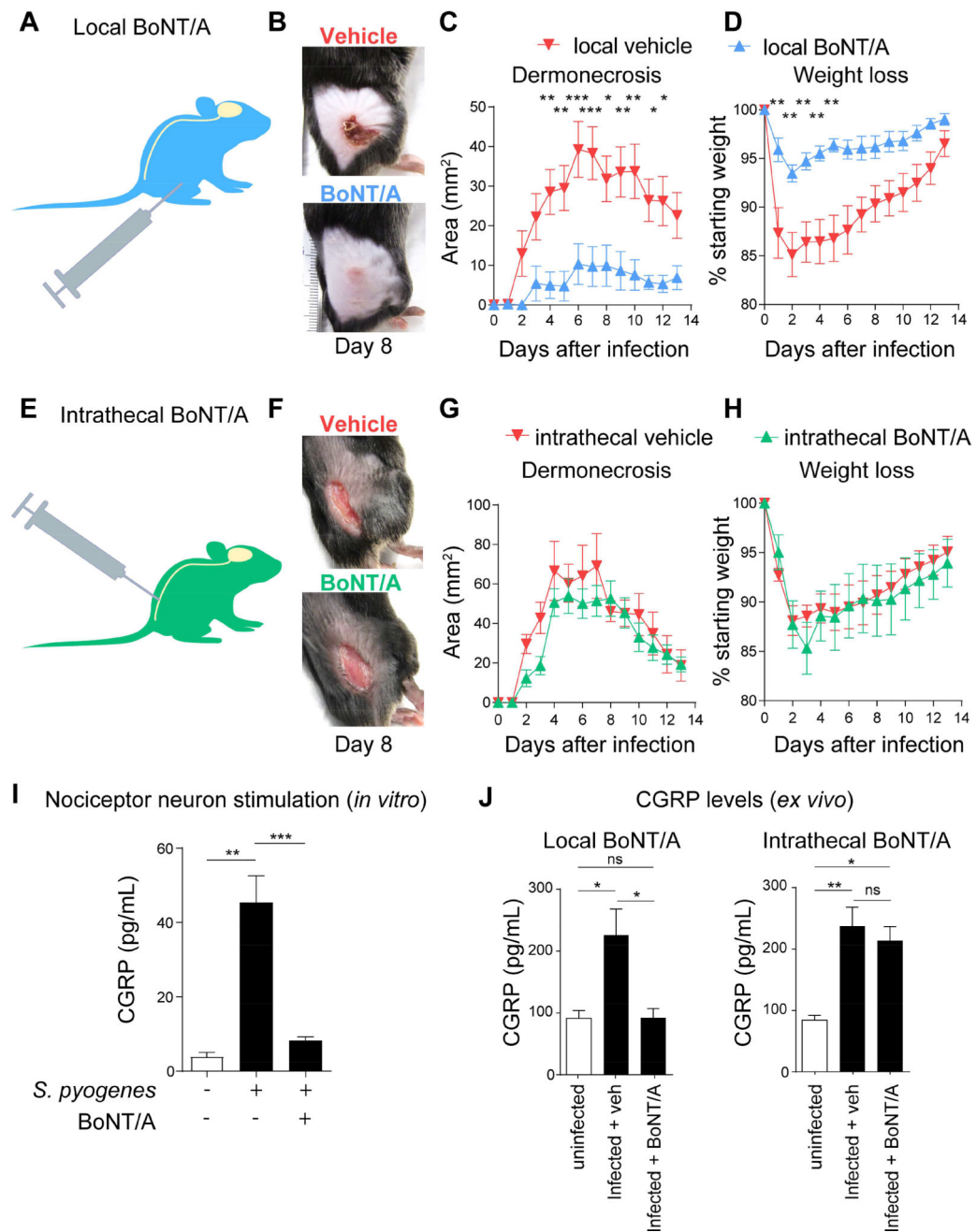


Figure 6. Local vs. intrathecal BoNT/A injection dissociates pain perception from peripheral neuro-immune suppression

(A–D) Subcutaneous administration of BoNT/A (25 pg/100 μ L) or vehicle 6 days prior to *S. pyogenes* M1 injection in flank skin (5×10^6 cfu). (B) Representative images of lesions (day 8), (C) Dermonecrosis size measurements, and (D) Weight loss over time after injection of *S. pyogenes* (n=5–10/group). (E–H) Intrathecal administration of BoNT/A or vehicle 1 day prior to *S. pyogenes* M1 injection in flank skin (5×10^6 cfu). (F) Representative images of lesions (day 8), (G) Dermonecrosis size measurements, and (H) Weight loss over time after injection of *S. pyogenes* (n=6/group). (I) DRG neurons exposed to BoNT/A (25 pg/200 μ L)

or medium for 24 h were stimulated with *S. pyogenes* supernatant (5×10^9 cfu/mL) for 30 min, and CGRP was measured in neuronal supernatant (n=5/group). **(J)** CGRP release from skin punch biopsies of mice treated intrathecally or locally with BoNT/A, 7 h after *S. pyogenes* M1 (5×10^6 cfu) injection (n=3/group). Statistical analysis: **(C,D,G,H)** Two-way ANOVA, Bonferroni post-tests. **(I,J)** One-way ANOVA, Tukey post-tests. *p<0.05 **p<0.01 ***p<0.001 ****p<0.0001. ns=not significant. Mean±SEM. See Figure S6 for related data.

Author Manuscript

Author Manuscript

Author Manuscript

Author Manuscript

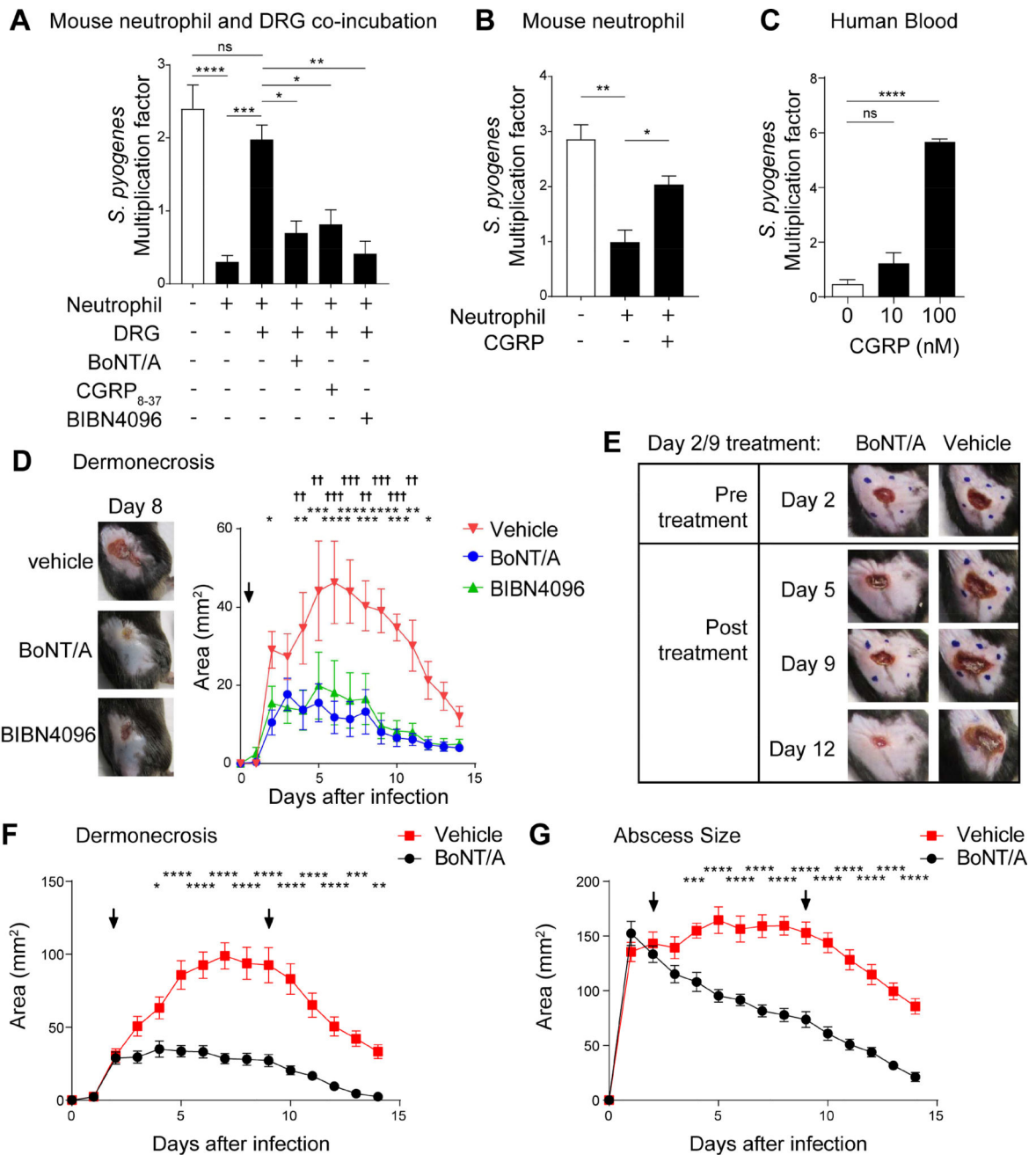


Figure 7. BoNT/A and CGRP antagonism block neural modulation of immunity to treat bacterial invasion

(A) DRG neurons were pretreated with BoNT/A for 24 h, or with CGRP antagonists (CGRP₈₋₃₇ or BIBN4096) immediately before co-incubation with mouse neutrophils and *S. pyogenes* M1 for 1 h. Bacterial survival was measured as the multiplication factor of surviving colonies/starting inoculum (n=3–4 replicates/group). (B) Mouse neutrophils were incubated with *S. pyogenes* M1 in presence of CGRP or vehicle for 1 h, and bacterial survival measured (n=4/group). (C) Human whole blood was incubated with *S. pyogenes* M1 in presence of CGRP or vehicle for 3 h, and bacterial survival measured (n=3/group).

(D) Representative images of lesions at day 8 (left) and dermonecrosis size (right) of mice treated 2 h after *S. pyogenes* M1 injection (5×10^6 cfu) with vehicle, BoNT/A, or BIBN4096 (n=6–7/group). **(E–G)** Mice were treated subcutaneously with BoNT/A or vehicle at day 2 and day 9 following flank injection of *S. pyogenes* M1 (5×10^6 cfu). Representative images show lesions before and after treatment **(E)**. Dermonecrotic lesions **(F)** and abscess sizes **(G)** were measured over time (n=10/group). Blue dots show injection sites at day 2 and day 9. Arrows show BoNT/A treatments. Statistical analysis: **(A–C)** One-way ANOVA, Tukey post-tests. **(D–G)** Two-way ANOVA, Bonferroni post-tests. **(A–C, F–G)** *p<0.05 **p<0.01 ***p<0.01 ****p<0.0001. **(D)** BIBN4096 vs veh: *p<0.05 **p<0.01 ***p<0.001 ****p<0.0001, BoNT/A vs veh: †p<0.05 ††p<0.01 †††p<0.001 ††††p<0.0001. ns=not significant. Mean±SEM. See Figure S7 for related data.